Alkali(ne earth) metal promotion in Ni-catalyzed thermal decomposition of methane

Master Thesis

S. (Stefan) Bismeijer

Daily supervisor:

MSc. S.E. (Suzan) Schoemaker

Examiners:

Prof. dr. P.E. (Petra) de Jongh

Dr. J.E.S. (Jessi) van der Hoeven

Materials Chemistry and Catalysis

Debye Institute for Nanomaterials Science

Utrecht University

Date:

April 2022 – May 2023

Materials Chemistry and Catalysis

Utrecht University

Abstract

To move towards a more sustainable form of energy production, CO_x emissions need to be drastically reduced. As renewable energy sources cannot yet provide for the growing demand, the thermal catalytic decomposition of methane could be a promising intermediate. Apart from energy-rich hydrogen, this reaction also adds value to the solid carbon by-product in the form of carbon nanostructures. Promotion with alkali and alkaline earth metals of Ni-based catalysts was investigated by following the carbon growth in-situ using a thermogravimetric analyzer. Nickel catalysts with Li, Na, K, and Mg as promoters were tested. It was found that under similar reaction conditions, all the promoters show different effects on the catalytic properties of the catalysts, with promotion by Na and Mg showing a large increase in both activity and lifetime. K, on the other hand, shows a reduction in both properties. For the Na-promoted catalysts a concentration dependency was found, suggesting that lower promotion concentrations are needed when going down the alkali metals. On the other hand, Mg-promotion showed a slight increase in catalytic performance when increasing the promoter concentration, this might suggest that the promoter effect of Mg is different from that of the alkali metals. Measurements performed at different temperatures found activation energies of 77, 83, and 102 kJ/mol for the tested Ni reference, Na-promoted, and Mg-promoted catalysts, respectively. Only for the Mg-promoted catalysts an optimum in the catalytic lifetime was found at around 450 °C. While the other two catalysts showed increasing lifetimes and total carbon yields with decreasing temperatures, where this was not expected. The formed carbon structures seem mostly unaffected by the introduction of the different promoters compared to the reference catalyst, suggesting limited changes in the carbon growth mechanism upon promotion.

Table of Contents

1. Introduction

1.1. General introduction

As the world is slowly starting to realize, we are currently in a major climate crisis. The earth's environment is drastically affected as the world is warming up. The major contribution to this global increase in temperature is the emission of greenhouse gasses emitted by the production of energy, which has been rapidly rising since the 1850s.[1–3] To combat these problems it is necessary to move away from the use of fossil fuels for our energy needs and switch to more renewable resources. Hydrogen has been proposed as a good alternative energy-dense fuel that can be used to produce energy without the release of greenhouse gasses, as it is oxidized to just water. Aside from the use of hydrogen as a fuel, it is also used in big quantities in the chemical industry, with the production of ammonia via the Haber-Bosch process as its biggest consumer.[4] While the use of hydrogen as a fuel might be an emission-free way of producing energy, the way hydrogen is currently being produced is not. As the infrastructure for green electricity needed to produce hydrogen by water electrolysis is not yet realized, most hydrogen is currently still produced using the steam methane reforming process.[5] Hydrogen is produced by the reaction of methane with water, but this reaction has carbon monoxide, as well as carbon dioxide as a byproduct.[6] For these reasons an alternative method of producing hydrogen without greenhouse gas emissions is needed. One method, proposed back in the 1990s by N.Z. Muradov, thermally decomposes hydrocarbons, instead of oxidizing them. This would result in hydrogen and solid carbon, instead of water and gaseous CO_x products, the reaction equation has been shown below.[7] Aside from the reduction in emissions, the solid carbon could also be a valuable product of this reaction instead of being a harmful gaseous by-product. Small industrial testing plants are currently being set up to take this process to industrial scales.[8]

$$CH_4\,(g) \rightarrow 2H_2\,(g) + C\,(s) \qquad \Delta H^0_{298} = 74.5\ \frac{kJ}{mol} \tag{1}$$

When catalysts are used to perform the thermal decomposition of, in the case of this work, methane, carbon nanomaterials are formed. These materials can take the form of fibers, nanotubes, with single or multiple walls, or other carbon nanomaterials.[9–12] These carbon nanomaterials have been shown to have very interesting properties and applications. Applications can be found in electronics, where for example carbon nanotubes can be applied in transistors.[10] They can also be used as starting materials for composites where strength and low weights are essential.[10] More environmentally impactful applications might include their use as adsorbents for pollutants or in functions like gas storage.[9,10,13] A final, but very interesting, application is the use of carbon nanostructures in catalysis. Here, they can mainly be used as catalytic supports due to their mesoporosity, high surface area, and specific metal support interactions. This can be an improvement over other carbon support materials, like activated carbon.[14,15] In some cases, carbon nanotubes, and nanofibers have even been used as direct catalysts. For example the oxidative dehydrogenation of ethylbenzene to styrene or methane decomposition.[16,17] All these different applications of the carbon product can add value to what, in the current energy production, is just an unwanted by-product.

For the catalytic thermal decomposition (CTD) of methane, different catalysts can be used. Most current research is being done on the upper-row transition metals, as they have higher availability and lower costs than other metals, while showing great activity in methane decomposition.[18] Of all upper row transition metals, Ni, Co, and Fe are the metals that have shown the best activity for this reaction. It has been reported that the catalytic activity increases when going from Fe to Co to Ni.[18–20] Multiple reasons why these metals show good activity for this reaction have been proposed. The first is their electronic structure, with a partially filled 3d orbital, which makes them able to accept electron density of the methane adsorbing on the surface. Dissociation is made possible by back donation from the

metal to the adsorbate, changing its electronic structure.[21] The carbon that is formed after dissociation is not deposited on the same sites where methane is dissociated. So the second reason that Ni, Co and Fe show good activity is that they are able to dissolve and transport carbon, which also frees up the dissociation sites.[21,22] The deposition of carbon happens by growing carbon structures. Currently, two ways of carbon growth have been reported in literature: Tip-growth, and base growth. Which of the two growth modes is favored during catalysis is mostly determined by the metal-support interactions. When the metal nanoparticles are weakly bonded to the support, the catalysis will yield tip growth, while strong interactions between the metal and the support will lead to base growth.[21,23] In both mechanisms, graphitic carbon is grown at the interface between the metal and the carbon nanostructure. While these mechanisms show a general method of how the CTD of methane works, research shows many different results in both catalytic properties, and in carbon products formed in this reaction. This is because the activity and formation of carbon products are dependent on many different parameters, of which the choice of metal is only one. Catalyst composition, morphology, catalyst preparation method, support used, pre-treatments, and catalytic conditions all play an integral role in the activity and the carbon nanostructure growth.[9,21,24]

In this work, the focus will be on Ni-based catalysts, as Ni has been shown to be the most active metal for this reaction. This high activity, however, also has a major drawback. As Ni-based catalysts still suffer from high deactivation rates, especially during catalysis at higher temperatures. This is mostly due to encapsulation of the Ni nanoparticles by carbon, which in turn blocks the active sites for methane dissociation and deactivates the catalysts.[24,25] The main way in which researchers are currently trying to combat this fast deactivation of Ni catalysts, is by combining them with different metals. These metals can be incorporated into the Ni-nanoparticles, by for example alloy formation, to induce structural, geometrical, and electronic changes in the particles. These bimetallic and sometimes even trimetallic catalysts have shown to be very beneficial in improving the catalytic properties of Ni-based catalysts.[24,26] Many different bimetallic catalysts have already been researched for this reaction, including combinations of the three main transition metals Ni, Co, and Fe, as well as Ni in combination with other metals.[27–29] Beside the three upper-row transition metals, other metals have been incorporated into Ni catalysts as well. Two examples are Cu and Pd, with Cu incorporation being the most notable, although both combinations have improved the lifetime and the activity of the researched catalysts for their respective studies.[25,30] Of all these bimetallic combinations, NiCu catalysts have gained much attention from the scientific community. While Cu does not show any activity for the CTD of methane by itself, the incorporation within Ni-based catalysts does improve the catalytic properties, hinting at structural or physical changes of the Ni particles having large effects on the catalysis.[18,25,26,31,32] The main explanations for these improvements are reported to be easier reducibility of the metal nanoparticles, better metal dispersions, and higher rates of methane adsorption. In addition to these factors, Cu also seems to improve the diffusion of carbon through the metal nanoparticles, and this affinity of Cu with the carbon nanostructures seems to be a key factor in reducing the encapsulation of the particles leading to deactivation.[24–26] This is in contrast to the solubility of carbon in NiCu alloys, as this has been reported to decrease with increasing Cu content, so the increase in carbon diffusion must compensate for the decrease in solubility.[33] These results on bimetallic catalysts, show not only that the catalytic properties of Ni-based catalysts can be improved upon addition of other elements within the catalyst composition, but also the importance of the change in physical properties that these promotional effects induce. In addition to these catalytic improvements, the carbon structures are affected due to this bimetallic functionalization. Showing, for example, the formation of carbon fibers with or without hollow cores depending on catalytic conditions, which might be directly related to the diffusion pathways through the catalyst particles.[9,31]

This is shown in figure 1. In contrast to NiCu catalysts, the formation of branched carbon fibers was shown for the bimetallic Ni-Pd system.[30]

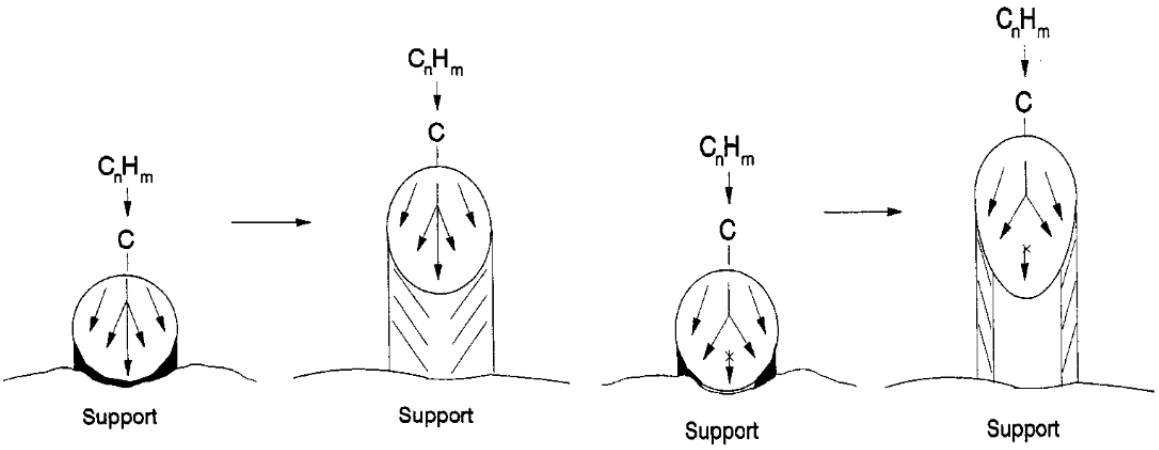

Figure 1: Schematic representation of the formation of a solid fiber (left) and a hollow fiber (right). (Adopted from Ref. 8).

As mentioned before, a large amount of research has already been done on the modification of Ni-based catalysts using bimetallic systems. Aside from this method of promotion, where structural and geometrical modification of the metal nanoparticles plays an important role, other types of promotion have seen less attention for this reaction. The promotion of alkali and alkaline earth metals has not been very well researched in the case of the CTD of methane.[34] In many other reactions this type of promotion has been shown to have either positive promotional effects, which increase catalytic properties, or harmful poisonous effects leading to less efficient catalysts.[35,36] The most famous example being the activation promoter K_2O, which is used for the industrial Fe catalysts, needed for ammonia synthesis. Without this promoter the use of this catalyst would not be viable on an industrial scale.[35,37] Other major reactions where this type of promotion has shown positive effects include the Fischer-Tropsch synthesis, methane steam reforming process, and dry methane reforming. In the case of the Fischer-Tropsch reaction, sodium and sulfur incorporation increased the activity of the reaction and boosted the selectivity towards the lower olefin fraction, while decreasing selectivity towards unwanted methane.[38] In the methane steam reforming process, coke formation could be reduced, by the addition of small amounts of K, which resulted in increasing lifetimes of the tested catalysts.[39] Lastly, dry methane reforming also showed decreases in coke formation through the addition of alkaline earth metal oxides e.g., MgO, CaO, and BaO. The addition of these promoters was also shown to increase the reducibility of these catalysts.[40,41] Beside the alkaline earth metals, the alkali metals have also shown promotional effects in dry methane reforming. Here the main effect seems to be on occupying the sites where coke is normally deposited.[42,43] This mostly leads to an increased in lifetime while reaction rates are less effected. This indicates that the type of promotion is less related to electronic effects, and more on the positioning of the promoter atoms. Because carbon encapsulation and fast deactivation is the main drawback limiting Ni-based catalysts, these promoter interactions, might improve the catalytic properties if similar effects are induced in the thermal catalytic decomposition of methane.

Some research has already been performed on alkali and alkaline earth metal promotion for the CTD of methane. Hussain et al. reported an increase in H_2 production, together with a decrease in carbon formation on the catalyst surface, through the addition of K to the NiCu/Al catalysts. Aside from this, they found an increase in lifetime for the K-doped samples. Multiple K concentrations were also tested for the catalysts and it was observed that at higher K concentrations the activity of the catalysts decreased sharply after several hours, indicating a concentration dependency on this type of

promotion.[44,45] Zapata et al. illustrated the effects of Ce, Ca, and K on silica-supported Ni catalysts, only finding a positive promotional effect for the cerium-promoted catalysts, where continuous activity was found due to the prevention of active site blockage by the formation of coke. K and Ca showed to negatively affect catalysis,[46] however, as a concentration dependency for K was found by Hussain et al. this might be the cause for this difference in findings. Lithium has been studied as a dopant by Musamali et al. The work shows high loading 37.5%Ni-12.5%Li/CaO catalysts, which showed better performance than monometallic 50%Ni/CaO catalysts for the CTD of methane. In the catalysis described, multi-walled carbon nanotubes, as well as carbon nanofibers are formed.[47] Finally, some work has been performed on the direct influence of Na promotion on the carbon nanostructures formed in the CTD of methane. Enlarging the inner diameter of carbon nanotube cores was found by the addition of Na_2CO_3.[48]

Beside from the work mentioned above, not much insight has been gained into the addition of promoters from the alkali and alkaline earth metal groups on Ni catalysts used for the CTD of methane. Within the continuation of this work, we will try to get a clearer view of how these promoters affect both the catalytic activity and lifetimes, as well as the formation of carbon.

1.2. Approach

To gain more insights into the effects of alkali and alkaline earth metals on the Ni-catalyzed CTD of methane, we will be synthesizing different promoted Ni-based catalysts. In the choice of catalyst for this research, many different factors need to be taken into consideration. As mentioned in the general introduction, both the support and the preparation method influence the final catalytic performance of the finished catalysts. To make sure that all prepared catalysts would be comparable to each other, all catalysts were prepared using the same method. Because the used support has been shown to have a significant influence on the catalytic properties of the catalysts, a support was chosen that reduced these support effects.[49–51] In our case, graphitic carbon was used due to its good thermal stability at the reaction conditions and only showed weak metal-support interactions.[52–54] Another advantage of this choice of support was the visibility of the different catalyst components while measured using electron microscopy. The reason for this is the low molecular weight of C giving better contrast to the Ni particles than metal oxide supports would. Lastly, separation of the products from the support would not be necessary as the carbon support would only make up a small portion of the final carbon product after catalysis. This would only leave the removal of the metal and reduce the harsh treatments needed if other more difficult-to-remove supports had been used. As this choice of support has weak metal support interactions, the tip growth mechanism of the carbon structures is to be expected.[31]

To deposit both the Ni and the promoter precursors onto the support material, multiple methods could be employed. In this work, we choose to apply an incipient wetness co-impregnation method as this method provided a way to deposit a precise amount of both Ni and promoter precursor onto the support at the same time. This is advantageous as pre-treatments to incorporate the promoter on the support, can lead to loss of pore volume, making it harder to obtain similar Ni loadings onto the final catalysts. The precursor salts used for impregnation were nitrates for the Ni, as well as for the promoters. $Ni(NO_3)_2 \bullet 6H_2O$ was chosen as it can be decomposed into NiO under relatively mild conditions without the need for any oxidizing gasses.[55] To make sure not too many different compounds were present in the precursor solutions, which could lead to unexpected reactions, the nitrate salts of the promoters were used, together with small amounts of nitric acid to acidify the solution to approximately pH 1.

To end up with catalytically active metal nanoparticles, the impregnated catalysts will have to be dried, heat treated, and reduced. For the heat treatment, no oxidizing agents should be needed as the Ni

precursor decomposes into NiO in inert atmosphere as well. Therefore, this will be done in just an N_2 flow, with heat treatment temperatures being determined using thermogravimetric analysis coupled with mass spectrometry (TGA-MS). For the reduction, both an ex-situ and an in-situ reduction were decided upon. The ex-situ reduction should make sure that a big part of the NiO has already been reduced before the catalysts enter the catalytic setup, ensuring an easy and complete reduction during the in-situ reduction step. This reduction step is deemed very important as a full reduction to metallic Ni needs to have occurred for all catalysts to be able to compare them accurately. Reduction temperatures were determined using temperature-programmed reduction coupled to a mass spectrometer (TPR-MS). At critical stages in the preparation of the catalysts, as well as after the catalysts were fully prepared, all catalysts were characterized using Inductively coupled plasma optical emission spectroscopy (ICP-OES), powder X-ray diffraction (XRD), nitrogen physisorption and (scanning) transmission electron microscopy ((S)TEM), occasionally in combination with energy dispersive X-ray (EDX). This was done to ensure a correct catalyst synthesis and to determine if the different catalysts could be accurately compared.

The chosen promoters to research for this work were Li, Na, K, and Mg. The alkali metals were used as they already have been shown to exhibit interesting effects on Ni-based CTD catalysts. However, the understanding of these promoters is still limited. Furthermore, no study has yet been carried out with all three alkali metals, in which they can be directly compared to one another to determine if any trends can be found when going down the first period. Mg has been chosen as the last promoter from the alkaline earth metals, as Ni supported on MgO has already shown interesting metal support interactions for the CTD of methane.[50,56] It would be interesting to determine if these effects are also present when Mg is used in smaller quantities as a promoter instead of as a catalyst support. It is also known that Mg can interact with Ni by the formation of alloys in both the metallic phase and its oxidized MgO phase.[57,58] Researching this could lead to interesting results and might show different kinds of promotion in comparison with the alkali metals. Finally, Li and Mg have been reported to have more similar properties than Li has with the other alkali metals, due to their isodiagonal relationship.[59] Making it an interesting addition to the three alkali metals being tested.

To determine the catalytic performance, catalytic testing was performed on a TGA-MS system. This system was combined with a gas mixing device to allow the use of hydrogen and methane for the in-situ reduction and catalysis respectively. Catalysis was performed in methane mixed with argon. Using the TGA system during catalysis, we were able to measure the reaction process in-situ, as the carbon formed in the reaction is deposited in its solid form, making it possible to measure the weight increase in the TGA during the catalytic reaction. From this data, it was possible to extract specific reaction parameters that will be presented and discussed in the results and discussion section.

Apart from measurements on all the catalysts promoted with the different elements mentioned above, we will also try to determine dependencies on the promoter concentration and catalytic temperatures for two of the promoters. Na- and Mg-promoted catalysts were chosen for this, as preliminary results showed good activities for these catalysts, and it was expected that slight changes would be easier to determine using more active catalysts. The concentration dependency was deemed interesting, as previous research mentioned in the general introduction showed different results for the same promotors used, and some dependency on the concentration was already observed.[44–46] The different temperatures were chosen as this would lead to the possibility of determining the activation energies for the different promoted catalysts. Aside from this, prior research showed a very big dependence on the temperature for NiCu catalysts, to where it was even proposed that the reaction mechanism changed upon differentiation of the catalytic temperature.[31]

To determine what kinds of carbon nanostructures are being formed during the catalytic measurements of the different promoted catalysts, TEM imaging is used. The images made on the microscope can be analyzed using image analysis software to obtain information on the type of structures formed, as well as on the size of these formed structures.

Using this approach, we will try and answer several questions in this work on the promotional effects of alkali and alkaline earth metals on the Ni-catalyzed thermal decomposition of methane:

- *How does the promotion with Li, Na, K, and Mg of Ni/C catalysts affect the activity and lifetime of these catalysts in the thermal decomposition of methane at 500°?*
- *How does the promotion with Li, Na, K, and Mg of Ni/C catalysts affect the carbon structures being formed during the thermal decomposition of methane?*
- *Is there any dependence on the concentration or temperature when promoting Ni/C with Na or Mg for the thermal decomposition of methane?*
- *Can any trends be found between the promotional effects of Li, Na, K, and Mg when used to promote Ni/C catalysts for the thermal decomposition of methane?*

Due to the limited research already performed on this type of promotion for the CTD of methane, it is hard to hypothesize what the answers to these questions will be. However, it is expected that the promotion will have a significant influence on the catalytic properties of these reactions, as this type of promotion has already been shown to cause severe changes for other reactions. Although, for other reactions the results of this type of promotion have not been found to follow a specific trend, it has been shown that the surface energy of the nanoparticles plays an important role concerning the formation of carbon structures.[21] Where alkali metals are mainly shown to affect this surface energy, it is expected that changes in the carbon structures will be observed.[21,34] On the topic of the dependence on concentration and temperature, the hypothesis is that these are indeed present and also very important. Because the electronic properties of the alkali and alkaline earth metals are quite strong, too much or too little might induce too much or too little change on the electronic structure of the Ni surface respectively. In the case of temperature, the catalytic properties usually change when going to lower or higher temperatures, leading to slower or faster deactivation. Whether this dependency will be the same for the different promotors, is still unclear. Since other trends have not yet been observed by other research for this type of promotion in this reaction, it is hard to make any predictions on that part. It would however be logical that as the electronic properties of the alkali metals get more extreme when going down the periodic table, the promotional effects that these additions impart on the catalysts will also get more extreme.

2. Experimental methods

2.1. Catalyst synthesis

Catalyst precursor solutions were prepared using three different components: promoter stock solution, the Ni precursor and nitric acid. Promoter stock solutions were made by dissolving required amounts of promoter nitrate salts ($LiNO_3$ (Sigma Aldrich), $NaNO_3$ (Thermo Scientific), KNO_3 (Sigma Aldrich) and $Mg(NO_3)_2 \bullet 6H_2O$ (Acros Organics) in 5 mL H_2O to obtain stock solutions with 0.875M promoter. The appropriate amounts of $Ni(NO_3)_2 \bullet 6H_2O$ (Sigma Aldrich) were dissolved in minimal amounts of water. To which the promoter stock solution and HNO_3 were subsequently added before the addition of water in a 5 mL measuring flask. Through this method, transparent green precursors with 3.5 M Ni, 0.35/0.175/0.117/0 M promoter and 0.1 M HNO_3 were obtained. The exact used quantities of the components for all catalysts can be found in Appendix 1.

The precursor solutions were deposited on the GNP500 (xGnP®C-500, XG Sciences) by incipient wetness co-impregnation. This was done by first drying the support for 2h at 170°C under vacuum while stirring. Afterward, 90% of the pore volume of the dried support was filled with precursor solution, by dropwise addition of precursor solution to the support at lowered pressure while continuously stirring to homogenize the sample. The impregnated catalyst was left to stir for another hour before being dried overnight under dynamic vacuum to evaporate the water in the precursor.

Using this method, catalysts with an atomic ratio of Ni to promoter of 20/1 were prepared for all different promoters. Catalysts promoted with Na and Mg were also prepared with atomic ratios of 10/1 and 30/1.

In the continuation of this thesis, the different catalysts will be depicted using their atomic ratio of nickel to promoter followed by Ni'promoter' e.g., 20NiNa for a Ni catalyst promoted with Na in an atomic ratio of 20/1 Ni to Na. All different catalysts used can be found in Appendix 1.

Decomposition of the precursor salts to oxides was achieved by heat treatment of the catalysts under inert N_2 atmosphere. Heat treatment was performed at 330°C for 3 hours with 200 mL/min·g_{cat} N_2 flow. A following reduction step was performed to reduce NiO to metallic Ni. This was done at 350 °C for 3 hours in 5% H_2 in N_2 at a constant flow of 200 mL/min·g_{cat}. Both treatments were performed in a glass reactor, hanging in a wire oven, with the flows coming from above. After reductions samples were left to slowly passivate in the air.

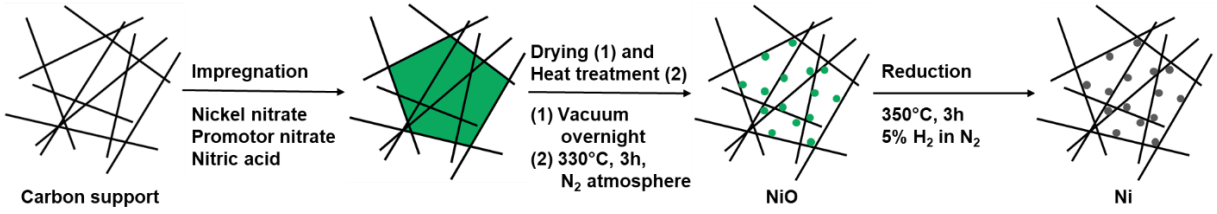

Figure 2: Catalyst preparation procedure, starting with the impregnation of the catalyst precursors. This is followed by a drying and heat treatment step to obtain NiO nanoparticles. At last, the samples are reduced to provide metallic Ni particles.

2.2. Catalyst characterization

TGA-MS

Thermogravimetric analysis coupled with mass spectrometry (TGA-MS) was performed on a TA Instruments TGA Discovery 5500 coupled to a TA Instruments Discovery II Mass Spectrometer, using platinum sample pans and balance and sample flows of 20 mL/min and 50 mL/min, respectively. To determine the decomposition characteristics of the precursor salts, first, a one-hour flushing step was

done to make sure the system was in inert argon atmosphere. thereafter, the sample was heated up (5 °C/min) to 500 °C, still under argon atmosphere, during which m/z 1-75 were measured using the MS system with a sample time of 1.8 seconds. TGA-MS measurements were performed on all impregnated and dried catalyst samples, with around 5 – 10 mg of catalyst per measurement. The evolution of the weight was transformed by differentiation against the temperature to obtain the weight change/°C. This data was coupled to the corresponding MS data when appropriate.

XRD

Powder X-ray diffraction (XRD) was performed using a Bruker D2 phaser in which a Co Kα source was utilized. Measurements were done with a deep ridged bottomed holder when enough sample was present, or a shallow flat-bottomed holder for smaller amounts of catalyst. Diffractograms were measured of all heat-treated, and reduced and passivated catalysts, as well as reference materials, from 2θ= 20-80°, at a step size of 0.01° and a measurement time of 1 sec per step. A variable rotation of the sample holder of 15°/min was used.

TPR-MS

Temperature Programmed reduction coupled with mass spectrometry (TPR-MS) was used to determine the reduction characteristics of the heat-treated catalysts. These measurements were performed on a Micromeritics AutoChem II 2920 with a Thermal Conduction Detector. The MS system used was a Hiden analytical QGA. All measurements followed the same method where approximately 50 mg of catalyst, sieved at a fraction above 75μm, was loaded into the quartz reactor in between layers of quartz wool. After loading the reactor in the setup, the sample was heated to 120°C at 5°C/min in argon and left to dry for 15 min. The sample was then cooled to ambient temperature before the gas was switched to 5% H_2 in argon (Linde). This was left to equilibrate for 10 minutes, after which the measurement was started. 15 minutes after the start of the measurement the sample was heated to 600°C with a ramp of 5°C/min. After another 11-minute wait, the measurement was stopped, the gas was switched back to pure argon and the sample was left to cool back to ambient temperature. During the entire measurement, the MS was used to sample the outgoing gas every 14.5 seconds, measuring the following m/z values: 2 (H_2), 17(NH_3), 16 (CH_4), 18 (H_2O), 28 (CO), 30 (NO), 32 (O_2), 40 (Ar), 44 (CO_2/N_2O).The measured TPR signals were converted to hydrogen concentrations using calibration 292_0104, measured on 31-01-2023.

From the plotted TPR data, the areas underneath the curves were integrated, and using this data the experimental H_2 uptake was calculated by Equation 2: shown below. Furthermore, the theoretical H_2 uptake was also calculated using Equation 3.

$$Experimental\ H_2\ uptake\ \left(\frac{mmol}{g}\right): \frac{A_{TPR}\left(\frac{cm^3}{g}STP\right) * p\ (atm)}{R\ \left(\frac{cm^3 * atm}{K * mol}\right) * T\ (K)} * 10^3 \quad (2)$$

in which A_{TPR} is the area underneath the TPR graph, p is the standard pressure, R is the gas constant and T is the standard temperature set at 298.15 K.

Equation 3 shows the theoretical H_2 uptake calculated from the amount of Ni present in the different catalysts.

$$Theoretical\ H_2\ uptake\ \left(\frac{mmol}{g}\right): \frac{0.01 * wt.\%\ NiO}{M_{NiO}\ (\frac{g}{mol})} * molar\ ratio\ \frac{H_2\ (mol)}{NiO\ (mol)} * 10^3 \quad (3)$$

with weight % (wt.%) NiO, the amount of NiO present in the catalysts, M_{NiO} the molar mass of NiO, and molar ratio the amount of H_2 needed to reduce NiO.

Electron microscopy

For the determination of Ni particle sizes, the distributions of Ni particles as well as promoters over the carbon catalyst support and the characteristics of the carbon products formed during catalysis, a combination of bright field Transmission electron microscopy (TEM) and High Angle Annular Dark Field (HAADF) images with Energy Dispersive X-ray (EDX) was used. Both imaging techniques were performed on an FEI Talos F200X electron microscope. TEM samples were prepared by first dispersing a small amount of catalyst or reaction product in absolute ethanol and sonicating this mixture for a short time. One or two drops of the resulting fine suspension were then pipetted onto a Cu grid coated with holey carbon (Agar Scientific 300 Mesh Copper grid). The acquired images were analyzed using ImageJ software, where around 300 particles were measured to obtain their size distribution, average particle size, and standard deviation. Carbon fiber products after catalysis were also analyzed using ImageJ to determine their width and fiber structure.

Physisorption

The pore characteristics of the catalysts were determined using nitrogen physisorption at 77K on a Micromeritics TriStar II Plus Version 3.01.01. Before the measurement, the samples were dried under vacuum at 170°C overnight. Around 65 mg of catalyst sample was used for the analysis.

ICP-OES

Inductively coupled plasma optical emission spectroscopy was used for the determination of the amount of Ni and promoter in the prepared catalysts. This was done on an Arcos Model Arcos spectro ICP-OES after microwave digestion on a CEM MARS 6. Measurements were performed on the catalysts after ex-situ reduction. These measurements were perfomed by MikroLab, mikroanalytisches laboratorium Kolbe.

2.3. Catalytic testing

Catalytic testing of the different promoted and unpromoted catalysts was done on a TGA-MS system. The apparatuses used were a TA Instruments TGA Discovery 5500 coupled to a TA Instruments Discovery II Mass spectrometer. To the TGA a TA Instruments Blending Gas Delivery Module was attached to allow the introduction of different gasses than Ar, and mixtures of these gasses, to the system. All experiments were performed using 100 µL platinum sample pans by TA Instruments and hydrogen (Linde) and methane (Linde, Methaan 5.5 Scientific 10L) in addition to Argon. Gasses other than Ar are only introduced in the sample flow. Measurements were done using 1-2 mg of catalyst sample, sieved in a size fraction from 75-150 µm, and all measurements were performed in duplo. The method of all measurements was as follows and is depicted in Figure 3: the method started with a flush of the system for 1 hour at 100-100 mL/min balance and sample flows of Ar to clear all the air out of the TGA oven and ensures an inert starting environment for the experiment, after which the balance and sample flows were again set to 20-50 mL/min respectively. The sample was then dried at 100 °C for 15 min followed by a reduction at 350 °C (5 °C/min) in 5% H_2/Ar for 3 h. The system was heated to reaction temperatures at 5°C/min, which varied from 450°C to 550°C for different experiments. When at reaction temperatures the system was left to equilibrate for 2 min. Methane was then introduced at 34% of the total flow, with the rest consisting of Ar. The reaction was performed for 30 to 240 min depending on the lifetimes of the different catalysts. After catalysis, the samples were cooled to ambient temperatures in a pure Ar flow.

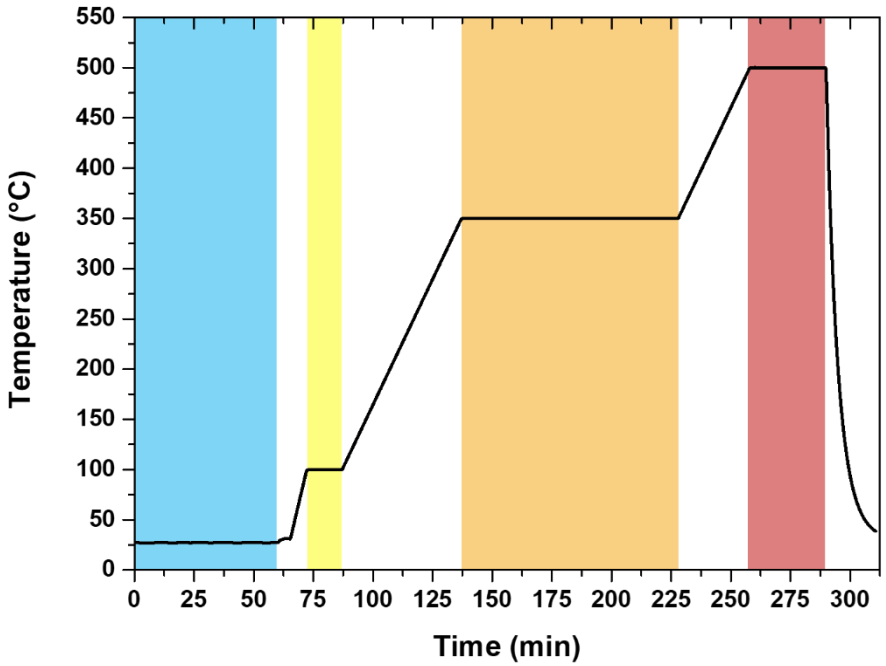

Figure 3:TGA profile for catalytic measurement with, in blue, flushing step with 100 mL/min argon balance and purge flows. In yellow, the drying step in 20-50 mL/min argon balance and purge flows respectively. In orange, the reduction step with a 20 mL/min argon balance flow and a 50 mL/min 5% H_2 in argon purge flow. In red, the catalytic step with a variable time and a 20 mL/min argon balance flow together with a 50 mL/min 34% methane in argon purge flow. The black line depicts the temperature profile over time.

2.4. Data Analysis

The catalytic data was analyzed using Origin software. Duplo measurements were averaged using: Average multiple curves. This was done over the full X range, with the creation of 300 points per half hour and linear interpolation. Standard deviations were calculated for these curves. The averaged curves were differentiated with a derivative order of 1 and a Savitzky-Golay smooth with a polynomial order of 2 and a window of 20 points was applied.[60] From the derivative curves the maximum growth speeds were determined. The lifetime was determined manually by determining the first point in the dataset where the carbon growth speed was less than 1% of the maximum growth speed. This time was then rounded down to two significant numbers, and an error of 10% was presumed. The total carbon yield was taken at the lifetime with the standard deviation calculated by the origin software.

For the catalytic measurements at 400°C, the lifetime was not reached within the measurement time. To approximate the lifetimes of these catalysts the growth speed curves were determined as mentioned above and these were fitted starting at X=40 using a linear (20NiNa and 20NiMg) or an exponential regression fit (Ni). Using the formulas created, additional points were extrapolated from which the lifetime could be approximated using the method above. The total carbon yield was approximated by integrating the growth speed. For these properties, the error was also presumed at 10%.

3. Results and Discussion

3.1. Catalyst characterization

The three main components of the catalyst preparation are the initial impregnation, the heat treatment, and the reduction. In this section, the theoretically calculated weight loadings will be compared with those measured by ICP, this is done as a measure of the success of the impregnation. During the heat treatment under inert conditions, the precursor salts are to be decomposed into an air-stable metal oxide form. This decomposition has been followed using TGA-MS and this will be discussed together with the actual effect of the heat treatment on the catalysts. During reduction, these oxides are reduced into their catalytically active metal variants and can be followed by TPR-MS, while the results of the reduction can be visualized using XRD. At last (S)TEM-EDX results will be shown with the determination of the Ni particle sizes right before catalysis together with the (promoter) distributions after reduction.

Catalyst synthesis

To determine if the incipient wetness co-impregnation resulted in the desired catalysts, elemental analysis was performed on all the reduced catalysts using ICP. Reduced catalysts were used as their composition would be closest to the composition during catalytic measurements. These results can be compared to the theoretical loadings of Ni and promoters, calculated from the precursor compositions and impregnated volumes.

Table 1: A comparison between the theoretically calculated wt% of Ni and promoters in the different catalysts and the by ICP measured wt% of Ni and promoters. Together with the BET surface area and total pore volume measured by N_2 physisorption at 77K.

	Theor. wt.% Ni	ICP wt.% Ni	Theor. wt.% promotor	ICP wt.% promotor	BET surface area (m^2 /g)	Total pore volume (cm^3 / g)
Ni	14.95	14.89	n/a	n/a	274	0.49
20NiLi	14.20	12.39	0.084	0.0814	299	0.42
10NiNa	14.66	14.11	0.57	0.53	285	0.54
20NiNa	14.61	14.35	0.29	0.28	280	0.43
30NiNa	14.31	14.04	0.19	0.21	286	0.47
20NiK	14.35	14.13	0.48	0.50	272	0.45
10NiMg	13.85	13.78	0.57	0.57	289	0.46
20NiMg	14.38	14.43	0.30	0.31	258	0.45
30NiMg	14.63	14.43	0.20	0.23	280	0.48

In Table 1, the theoretical and ICP data of the Ni and promoters can be found, together with the physisorption results of the catalysts. When comparing the Ni weight percentages between the theoretical calculations and the ICP measurements only small differences were found, except in the case of the 20NiLi catalysts. These small exceptions are not uncommon due to the human error in the synthesis procedure. The lower actual Ni content found by ICP in comparison to the theoretical values for the 20NiLi catalyst could be a result of different things. It might have been caused by a mistake made in the synthesis or the theoretical calculations. This, however, is seen as unlikely as the ICP wt.% of promoter does not display the same level of change between the theoretical and measured weight

percentages. Another explanation might be some inhomogeneity of the Ni over the catalyst sample, but this would be hard to determine without more measurements. A last explanation could be that during heat treatment and reduction, something different happened to the 20NiLi catalyst compared to the other catalysts, resulting in more compounds present in the precursor solution being left in the final catalysts, where this would not be expected. This point will be addressed again later in the section on reduction.

Since the loadings measured using ICP are considered the most accurate for the different catalysts, these values will be used in all calculations and transformations used in the rest of this thesis.

Heat treatment

TGA-MS was used to determine the temperature at which the metal precursors that are impregnated on the different catalysts would decompose. Whether the peaks measured in the TGA experiment result from the decomposition of the impregnated precursor salts, can be determined using the MS data.

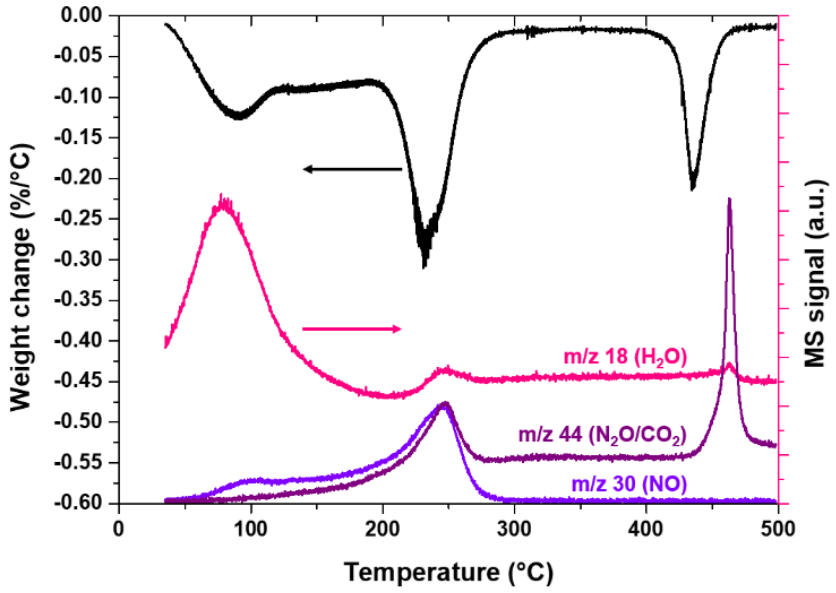

Figure 4: TGA-MS measurement of the Ni catalyst. The black line shows the derivative of the TGA profile and the colored lines show the MS signals of m/z 18, 30 and 44 in pink, purple and dark purple respectively.

In Figure 4 the MS data for m/z fragments 18 (H_2O), 30 (NO), and 44 (N_2O/CO_2) of the reference Ni catalyst can be found. The large H_2O signal nicely corresponds to the first TGA peak at 90°C with a small contribution of the N_xO_x signal. This first H_2O separation at lower temperatures corresponds to the thermal decomposition pathway of $Ni(NO_3)_2 \bullet 6\ H_2O$ published by Brockner et al. as can be found in

Water separation

1. $Ni(NO_3)_2 \bullet 6H_2O \rightleftharpoons Ni(NO_3)_2 \bullet 4H_2O + 2H_2O$
2. $Ni(NO_3)_2 \bullet 4H_2O \rightleftharpoons Ni(NO_3)_2 \bullet 2H_2O + 2H_2O$

Partial decomposition steps (oxidation and partial condensation)

3. $Ni(NO_3)_2 \bullet 2H_2O \rightleftharpoons Ni(NO_3)(OH)_2 \bullet H_2O + NO_2$
4. $Ni(NO_3)(OH)_2 \bullet H_2O \rightleftharpoons Ni(NO_3)(OH)_{1.5}O_{0.25} \bullet H2O + 0.25H_2O$

Decomposition

5. $Ni(NO_3)(OH)_{1.5}O_{0.25} \bullet H_2O \rightleftharpoons 0.5Ni_2O_3 + HNO_3 + 1.25H_2O$

Oxide decomposition to ''NiO''

6. $3Ni_2O_3 \rightleftharpoons 2Ni_3O_4 + 0.5O_2$
7. $Ni_3O_4 \rightleftharpoons 3NiO + 0.5O_2$

(4)

Equation 4.[55] Going to higher temperatures the MS signals of N_xO_x-fragments increase until the peak at 250°C after which the precursor should be fully decomposed to NiO, and the curves flatten out as expected. As the concentration of the promoter precursors was very low, the contribution of the promoter salts decomposition on the TGA profile is assumed to be negligible in contrast to the decomposition of the Ni precursor. The only TGA peak not fitting in this decomposition process is the peak at 440 °C., the MS data show a peak here of the m/z 44 fragment, but in contrast to the peaks at lower temperatures, there is no corresponding peak for the m/z 30 fragment. This would mean that the m/z 44 peak is not originating from N_xO_x but from CO_2. This leads us to believe that at higher temperatures the NiO is already being reduced to Ni, with the carbon support as the reducing agent in inert atmosphere. This is also shown to happen in literature with other metals supported on carbon.[61]

For all catalysts three distinct peaks can be observed at around 90 °C, 250 °C, and 440 °C. The decomposition profiles from the different catalysts can be found in the left graph of Figure 5. The full size TGA profiles with corresponding MS data are displayed in Appendix 2. 20NiLi is the only catalyst that shows a very big shift in one of the peaks, having the peak at ~440 shifted to 480 °C, this would mean that the addition of Li to the Ni catalysts lowers the autoreducibility of the NiO by carbon. The combination of these results led us to a heat treatment temperature of 330°C for all catalysts, as this is shown to lead to full decomposition of the precursors, but no reduction to metallic Ni.

The results of the heat treatment were analyzed using powder-XRD. The zoomed-in diffractograms can be found on the right in Figure 5, whereas the full diffractograms can be found in Appendix 3. The diffractograms show a characteristic NiO peak at 43° and a combined peak of NiO and the carbon support at 50.5°, while peaks at 52° and 61° indicative of Ni are not present. This confirms the success of the chosen heat treatment and the decomposition of the Ni precursor to NiO. It is still unclear in what states the promoters are present in the different catalysts. The Li and Mg nitrate salts are supposed to decompose into their oxide variant at elevated temperatures, while the Na and K nitrates are supposed to only decompose into their nitrite variants.[62–65]

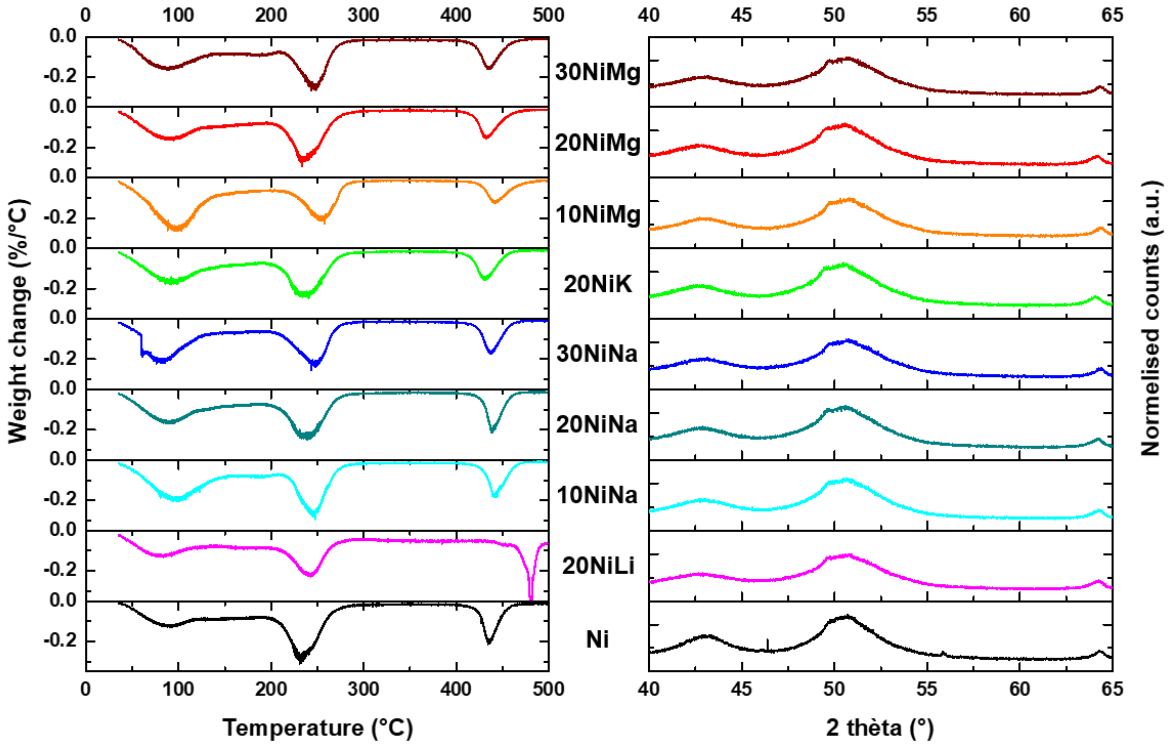

Figure 5: On the left the derivatives of the TGA profiles of all catalysts measured from 30 to 500°C at a ramp of 5°C/min in Ar flow of 50 mL/min. On the right the zoomed in XRD profiles of the different catalysts from 40 to 60°2θ. The XRD profiles were measured after the catalysts had undergone heat treatment at 330°C for 3 hours in a 200 mL min^{-1} g^{-1} N_2 flow.

Reduction

The determination of the temperature at which the NiO is reduced to metallic Ni was done using TPR-MS. As the metallic Ni nanoparticles are active as catalysts for the decomposition of methane to H_2 and carbon, they are also active for the methanation of carbon in the presence of H_2.[52] This means that the peaks H_2 uptake observed in the TPR profile, is a combination of the reduction of NiO to Ni and the methanation of the carbon support. Using MS, we were able to visualize the formation of methane as can be seen by the pink line in Figure 6, where the TPR profile of the Ni catalyst with the corresponding methane MS signal can be seen. In Appendix 4 TPR profiles with the corresponding methane signals of the other catalysts can be found. It can be observed that the methane signal corresponds with the position of the last peak seen in the TPR profile between 450 and 500 °C, but that methane is already measured starting from 250 °C. It was not possible to quantify the amount of H_2 that was taken up by the methane being produced because the MS system was not calibrated.

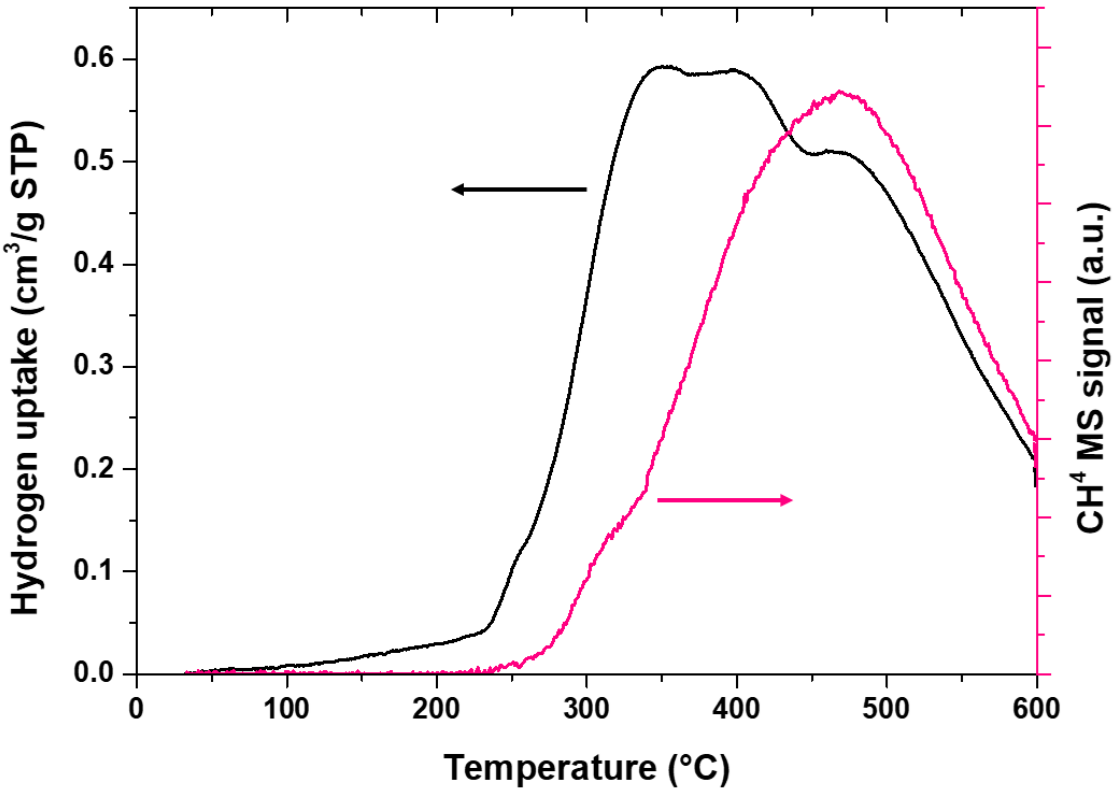

Figure 6: TPR profile of Ni catalyst (black), measured at a heating rate of 5°C/min in 5% H_2/Ar. In pink the corresponding MS signal of the methane fragment, measured at 14.8 second intervals.

With the third peak being assigned to the methanation of the carbon support, two peaks are left in the TPR signals for the catalysts to be assigned. These peaks are most likely both coming from the reduction of NiO. The peak at lower temperatures coming from Ni being more weakly bonded to the support than the signal at the slightly higher temperature.[66,67] As the carbon support does not have very strong Ni-support interactions the shift between these peaks is not very big.

When the theoretical amount of H_2 needed to reduce all the NiO in the catalysts is compared to the amount of H_2 taken up in the TPR experiments, which is calculated using Equation 3 and can be found in Table 2. It can be observed that for all catalysts the experimental H_2 uptake during the TPR measurement far exceeds the H_2 needed to fully reduce the NiO present in the catalysts. However, as the methane produced has not been quantified this cannot be said with certainty.

Table 2: Experimental and theoretical hydrogen uptakes for all different catalysts.

	T1 (°C)[1]	T2 (°C)[1]	A_{TPR} (ml/g_{cat} STP)	Experimental H_2 uptake ($mmol/g_{cat}$)[2]	Theoretical H_2 uptake ($mmol/g_{cat}$)[3]
Ni	100	600	147	6.0	2.4
20NiLi	100	600	142	5.8	2.3
10NiNa	100	600	143	5.8	2.4
20NiNa	100	600	117	4.8	2.4
30NiNa	100	600	138	5.6	2.3
20NiK	100	600	148	6.0	2.4
10NiMg	100	600	121	4.9	2.3
20NiMg	100	600	145	5.9	2.4
30NiMg	100	600	143	5.8	2.4

[1]T1 and T2 are the boundaries for the peak integration.
[2]A_{TPR} is the integrated area underneath the measured TPR curve.
[3]Experimental H_2 uptake calculated using Equation 2.
[4]Theorеretical H_2 uptake calculated using Equation 3.

For the other catalysts, the TPR profiles can be found in Figure 7. The figure shows that all the TPR measurements follow a similar profile as the one shown in Figure 6. Only the 10NiMg catalyst shows only two peaks instead of three. Nonetheless, it is suspected that these two peaks are still a combination of the three peaks found for the other catalysts.

The combination of these results led us to a reduction temperature of 350°C. This temperature showed high amounts of H_2 uptake corresponding to NiO being reduced to Ni for all catalysts. Additionally at this temperature, the formation of methane was still low compared to higher temperatures. A longer reduction duration of 3 hours was chosen to ensure full reduction of the NiO, as the temperature was chosen on the slightly lower side.

Powder-XRD measurements were performed after reduction and passivation. With passivation the partial oxidation of the reduced Ni in air is meant, as metallic Ni is not stable in the presence of O_2. The zoomed-in diffractograms can be found on the right side of Figure 7, with the full diffractograms found in Appendix 5. In contrast to the diffractograms shown before, which were measured after heat treatment, these diffractograms show that for most catalysts the combined peak at 50.5° has shifted to 52°. This is still a combined peak with the carbon support, but the shift to a higher 2θ is indicative of NiO being reduced to Ni. A second peak indicating the presence of metallic Ni can be found at 61°. This peak can also be found in all the diffractograms instead of the one from 20NiLi. Minor peaks for NiO can still be seen at 43° and 50.5°. As metallic Ni readily oxidizes in the presence of oxygen these peaks most likely relate to a layer of NiO formed on the surface of the Ni particles after passivation in air following the reduction.

As mentioned before, the 20NiLi catalyst does not show the shift in the combined peak with carbon or the Ni diffraction peak at 61°, found for the other diffractograms. When looking at the peaks for NiO at

43° and 50.5°, it can be observed that they are still present and are more intense than for the other samples. This would mean that the only phase of Ni present in the 20NiLi catalyst even after reduction is NiO. One explanation might be that the NiO was never reduced during the reduction process, however, this is unlikely as the TPR profile of the catalyst is very similar to that of the other catalysts. Additionally, the formation of methane during the TPR measurement indicates the presence of metallic Ni, as this is the active catalytic phase in the decomposition of methane and its reverse reaction.[68] Thus, it is reasonable to assume that the NiO has been reduced to metallic Ni during the reduction. However, this would mean that after reduction all the metallic Ni has again been oxidized to NiO, whereas for the other catalysts, this was only a partial oxidation. As such, the addition of Li to the catalytic system seems to influence the oxidation properties of the Ni nanoparticles. This might also explain the shift in the auto-reduction peak seen in the TGA profile of 20NiLi in Figure 5. How Li influences this oxidation and reduction behaviour would require further study, as other studies show different effects with Li-doped Ni catalysts.[69,70] Our results, however, might also be part of the explanation for the difference between the theoretical Ni loading and the ICP-measured Ni loading on this catalyst. As the Ni is fully in its oxidized state, the weight of this oxygen is included in the total sample weight used to determine the ICP wt.%, while this is not considered for the theoretical wt.%. When the theoretical calculations are done under the assumption that Ni is present in the catalyst as NiO, the theoretical wt.% will be 13.7% instead of 14.2%. This is slightly more in line with the ICP measurement, but still not the explanation for the large difference.

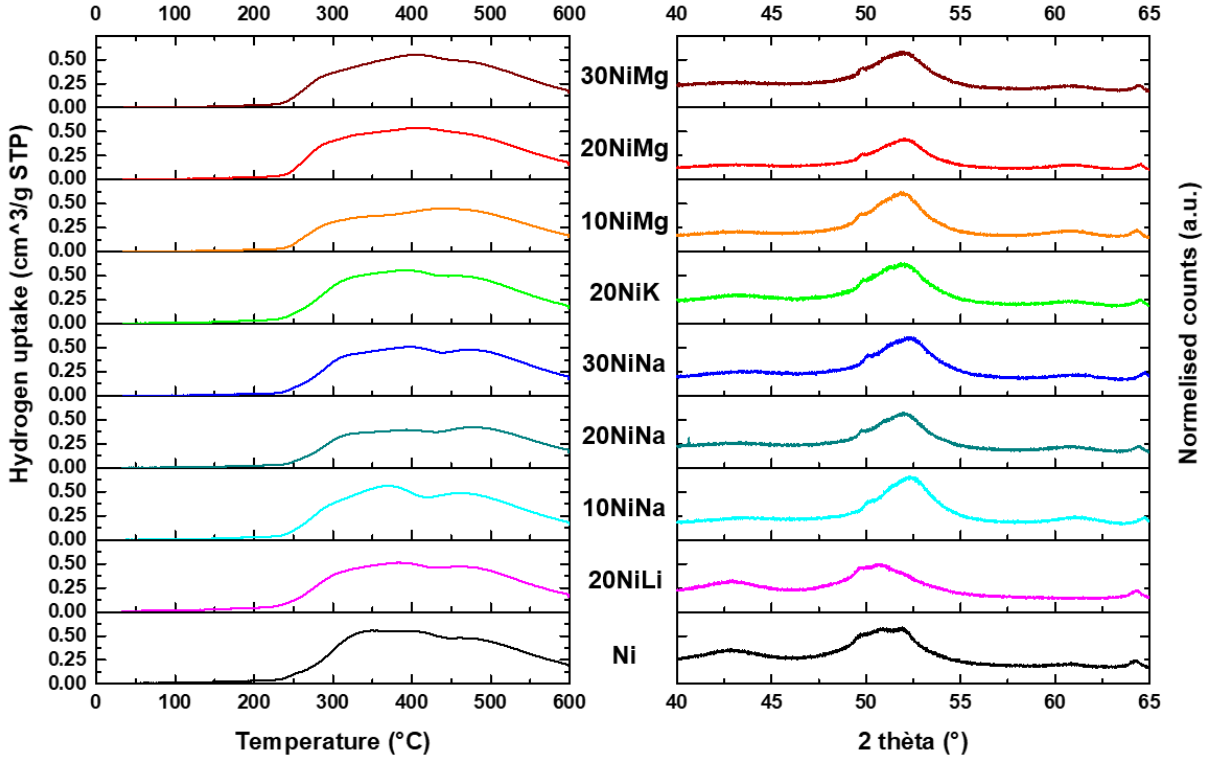

Figure 7: On the left, the TPR profiles for all the different catalysts measured from 30-500°C at 5°C/min in a 5% H_2/Ar flow. On the right the zoomed-in XRD diffractograms from 40 to 65° 2ϑ. The XRD diffractograms were measured after the catalysts had undergone reduction for 3 hours at 350°C in a 5% H_2/N_2 flow at 200 mL min^{-1} g^{-1} and had been passivated in the presence of air.

TEM-EDX analysis

To determine the distribution of particles covering the support surface as well as the sizes of these particles, TEM imaging was applied. All the catalysts characterized using TEM have undergone heat treatment and the ex-situ reduction, as well as the temperature and reduction program in the TGA, used for catalysis. Instead of performing catalysis, when the sample reached catalytic temperature after the in-situ reduction, the catalysts were cooled down. This ensures the imaged catalysts are as close to what they would be during catalysis as we could achieve, with them being reduced for a second time in situ and brought up to catalytic temperatures.

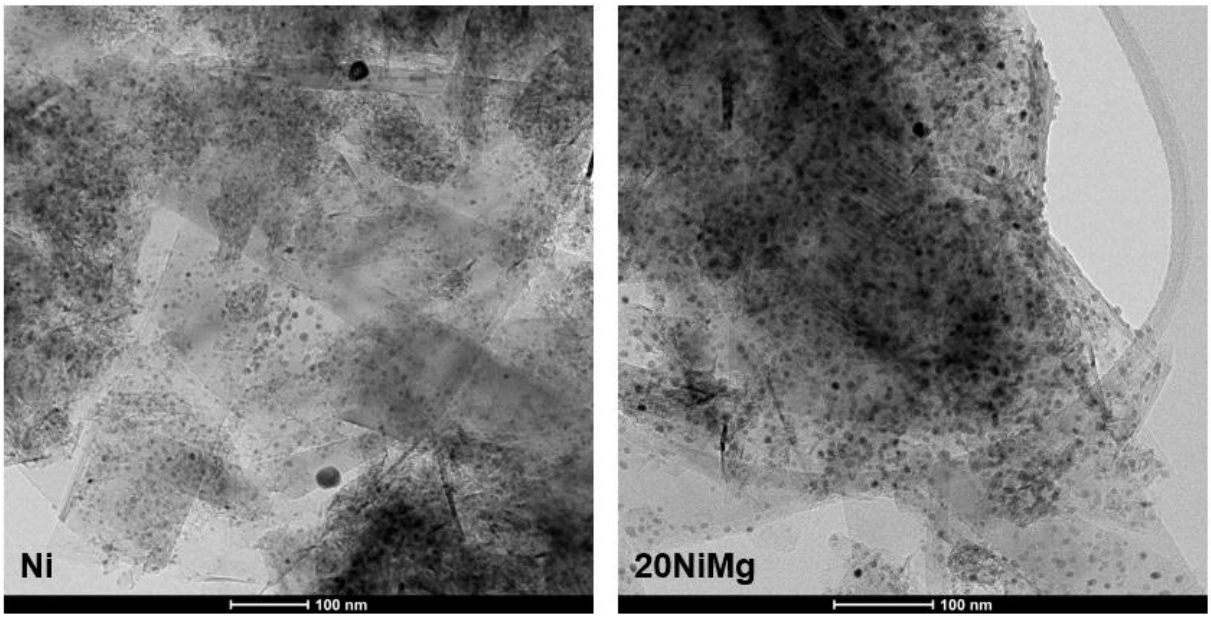

Figure 8: TEM images of the Ni and 20NiMg catalysts measured after in-situ reduction and heating up to catalytic temperature at 500°C in the TGA-MS system.

In Figure 8, two TEM images of the Ni and the 20NiMg catalysts are shown. These images clearly show a nice distribution of small particles over the carbon support with sporadic bigger particles among them. This homogeneous distribution of particles over the support can be found throughout all the different prepared catalysts. The particle size distributions (Appendix 6) also show that the bigger particles found for the catalysts shown in Figure 8 are also observed in the different catalysts. The average particle sizes with their standard deviations, shown in Table 3, are also very similar between the different samples, with the particles for the non-promoted Ni catalyst being slightly smaller than for the promoted catalysts. Because larger particles have been shown to have higher activities and lifetime in the CTD of methane,[71] this might be an indication that the promoted catalysts will have higher activities due to their larger particles at catalytic conditions. The similar particle sizes, between promoted catalysts, do lend themselves to good comparability of the effects of the promoters instead of the effects of particle sizes. The particle sizes measured from the catalysis done at different temperatures, will be discussed in section 3.2.3 along with the results of these measurements.

Table 3: Average particle sizes with their standard deviation for the different catalysts, acquired by the measurement of >300 particles per sample.

	Average particle size (nm)	Standard deviation (nm)
Ni	7.7	± 2.5
20NiLi	6.8	± 1.7
10NiNa	6.8	± 2.0
20NiNa	8.3	± 2.6
30NiNa	6.2	± 1.8
20NiK	8.0	± 2.1
10NiMg	7.3	± 2.7
20NiMg	8.1	± 1.9
30NiMg	7.1	± 2.3

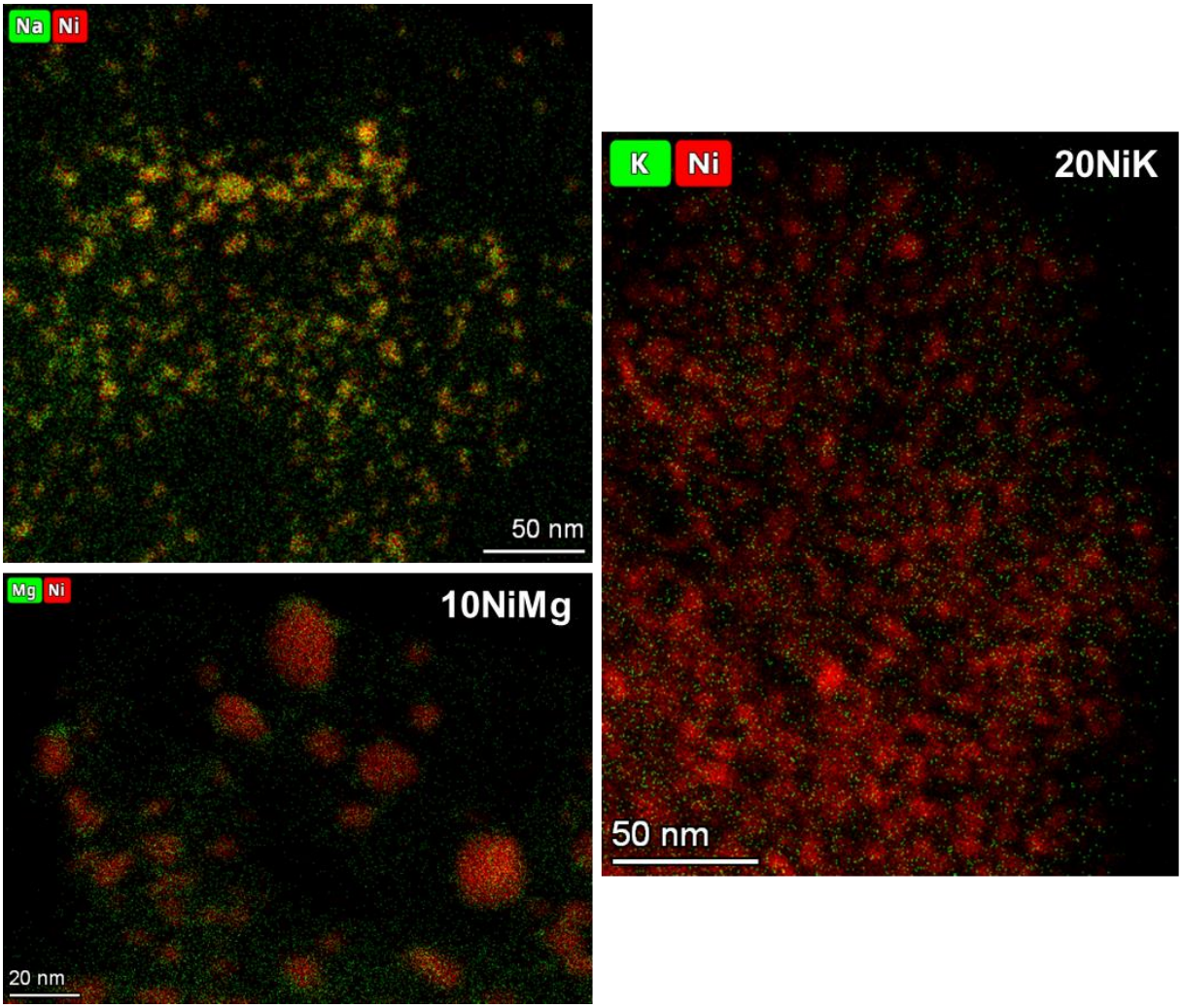

Figure 9: HAADF- STEM EDX images of the 10NiNa catalysts, with Na in red and Ni in green. The 20NiK catalyst with K in green and Ni in red, and the 10NiMg catalyst with the Mg signal in green and the Ni signal in red.

To determine at which positions in the catalysts the promoters are present, HAADF STEM-EDX was used on the catalysts after ex-situ reduction. Using this technique for the Li-promoted catalyst was not possible, as Li has too low of a molecular weight to be measured by the TEM that was used. Another limitation was the loading of the promoter on the other catalysts. A metal loading of 1% is normally applied as a minimum to be visualized using EDX. The promoter loadings for these catalysts are in a range from 0.2-0.6 wt.%, and thus the promoter locations can only be visualized when they are very well clustered together. To gain the best insight in the case of the Na- and Mg-promoted catalysts, the catalysts with the highest promoter loadings were used for this determination.

EDX maps of the 10NiNa, 20NiK, and 10NiMg catalysts, with the promoter signals shown in green and the signals from Ni shown in red, can be found in Figure 9. The Ni nanoparticles can be clearly distinguished as signal clusters. For the Na- and Mg-promoted catalysts, it can be observed that the promoter is more prominent around the Ni particles, while for the K-promoted catalyst, the density of the promoter signal seems evenly dispersed around the catalysts. The HAADF-STEM images corresponding to the EDX maps have not been shown as the signals become very difficult to distinguish. Nonetheless, the density of the promoter signal does seem contained to the support particles which indicates that the promoters are indeed present on the catalysts.

It is not entirely surprising that the promoter on the K-promoted catalysts seems to be spread out over the catalysts, as Li and K-ions have been shown to intercalate in layered graphitic carbon structures, which we use as the catalyst support, while Na and Mg do not show this behaviour in their ionic form.[72] However, the carbon support used is not a perfect graphite, in which intercalation occurs very readily, but a turbostratic graphite, in which intercalation is a lot harder.[73] Due to this, not much intercalation is expected. To determine if intercalated Li and K-species are formed, normally XRD is applied, as the interlayer spacing of the graphitic layers changes upon integration of alkali ions between them. However, due to very low promoter loadings and the non-perfect graphitic layering of the GNP500 support, this shift in the carbon peaks is not easily observable. To do this, the use of an internal standard could be used in the XRD samples to correct for slight differences in sample height.

3.2. Catalysis

After the characterization of all the catalysts, they were measured on the TGA-MS system for their catalytic properties in the thermal decomposition of methane. The weight of the sample was followed during the reaction, using this system, as it increased through carbon growth. Before the reaction, all samples were in situ reduced in H_2 and kept in inert atmosphere afterward to ensure the active metallic Ni-phase for the catalytic reaction. In the following sections, the results of the catalytic experiments will be presented and discussed. The main properties of the catalysts will be discussed in terms of total carbon yield, lifetime, and carbon growth speed. It will be attempted to link these different properties to different physical properties of the promoters to get a more fundamental insight into the alkali(ne earth) metal promoted reaction. In the first section of this chapter, the different promoted catalysts with a 20 Ni/promoter ratio will be compared at a set temperature of 500°C. After this, the focus will be put on two of the used promoters, Na and Mg, where the focus will be on the effect of the promoter concentration on catalysis, and different catalytic temperatures on the function of these catalysts. In all instances, the unpromoted Ni catalyst will be used as a reference to compare to the promoted catalysts. At last, we will have a look at the different carbon products that were formed to see if the different promoters and reaction conditions had any effect on the type of carbon structures that were formed during the reactions.

The validity of the measurements performed on the catalytic setup has been confirmed by blank measurements on the different variables that might influence the results. The results of these measurements can be found in Appendix 7. Measurements have been performed on empty sample pans to exclude any influence of the pans, at different flow rates to exclude diffusion limitations, and with different ways of loading the sample into the sample pan, also to exclude this affecting the gasses from diffusing to and into the samples. While these measurements all showed little to no effect on the catalysis, some of the duplo measurements of the catalysts still showed significantly large deviations. One possible reason for this that has not yet been explored is that the catalysis happens at harsher temperatures than the catalysts have undergone during the catalyst's synthesis, which would lead to changes in the catalyst during the catalytic experiments. This problem could be corrected by including a heat treatment at harsher conditions before catalysis to establish a stable catalyst structure during the whole catalytic measurement. As this problem at the time of writing has not yet been corrected, these large deviations will result in a large error on the averaged catalytic data for this work.

3.2.1. Different promoters

All the promoters used in this section have been measured during catalysis at 500 °C to make a fair comparison between the different promoters that were tested. The averaged evolution of carbon yield over time for the Na-, K-, Mg-, and un-promoted catalysts at 500 °C has been displayed in Figure 10a. The reference Ni catalyst is shown in black while the Na-, K-, and Mg-promoted catalysts are shown in cyan, green, and red respectively. From these measurements it's easily observed that the incorporation of the promoters has a very significant effect on the catalytic properties of the Ni catalyst. Under the used conditions both Na and Mg promotion seems to increase both the activity and the lifetime of the catalysts, while the K-promoted catalyst seems to have decreased in both activity and lifetime compared to the reference Ni catalysts.

When we look at the individual reaction properties of the catalysts: lifetime, total carbon yield and maximum growth rate, which are shown in Figure 10b, we see that the same trend is followed between the different parameters. The lifetime of the 20NiNa and 20NiMg catalysts is slightly higher than that of the reference Ni catalyst, whereas the lifetime of the K-promoted catalyst is lower. The same trends are observed for the total carbon yields and the maximum growth rate, with 20NiMg performing best. The highest lifetime for 20NiMg corresponds to both the highest total carbon yield as well as the

highest maximum growth rate. That the lifetime and carbon yield are correlated is quite logical, when the catalyst is active for longer, it has more time to grow carbon, which can lead to higher yields. A higher maximum growth rate together with a longer lifetime and a higher total carbon yield, would mean that the Mg- and Na-promoted catalysts can at least transport the created carbon faster, as otherwise, this higher growth rate would lead to faster deactivation. These results might also give an indication as to what type of promotion is present. The lifetime and subsequently the total carbon yield both seem to be most affected by the incorporation of the promoter, while the differences in the growth rate are not very large. This can indicate that electronic effects only play a minor role here, as this would have resulted in a larger impact in the growth rates. Because lifetime is most effected, it might be the case that the promotional effects are more like those seen in dry methane reforming. Here the alkali- and alkaline earth metal promoters are present on the sites where coke is deposited.[40–43] As this coke deposition leads to deactivation of the catalysts, lifetime is increased when this coke deposition is inhibited. As the deposition of amorphous carbon is also the main deactivation mechanism for these catalysts, the same effect might be observed here. Determining the precise positioning of the promoters would be very important to confirm this.

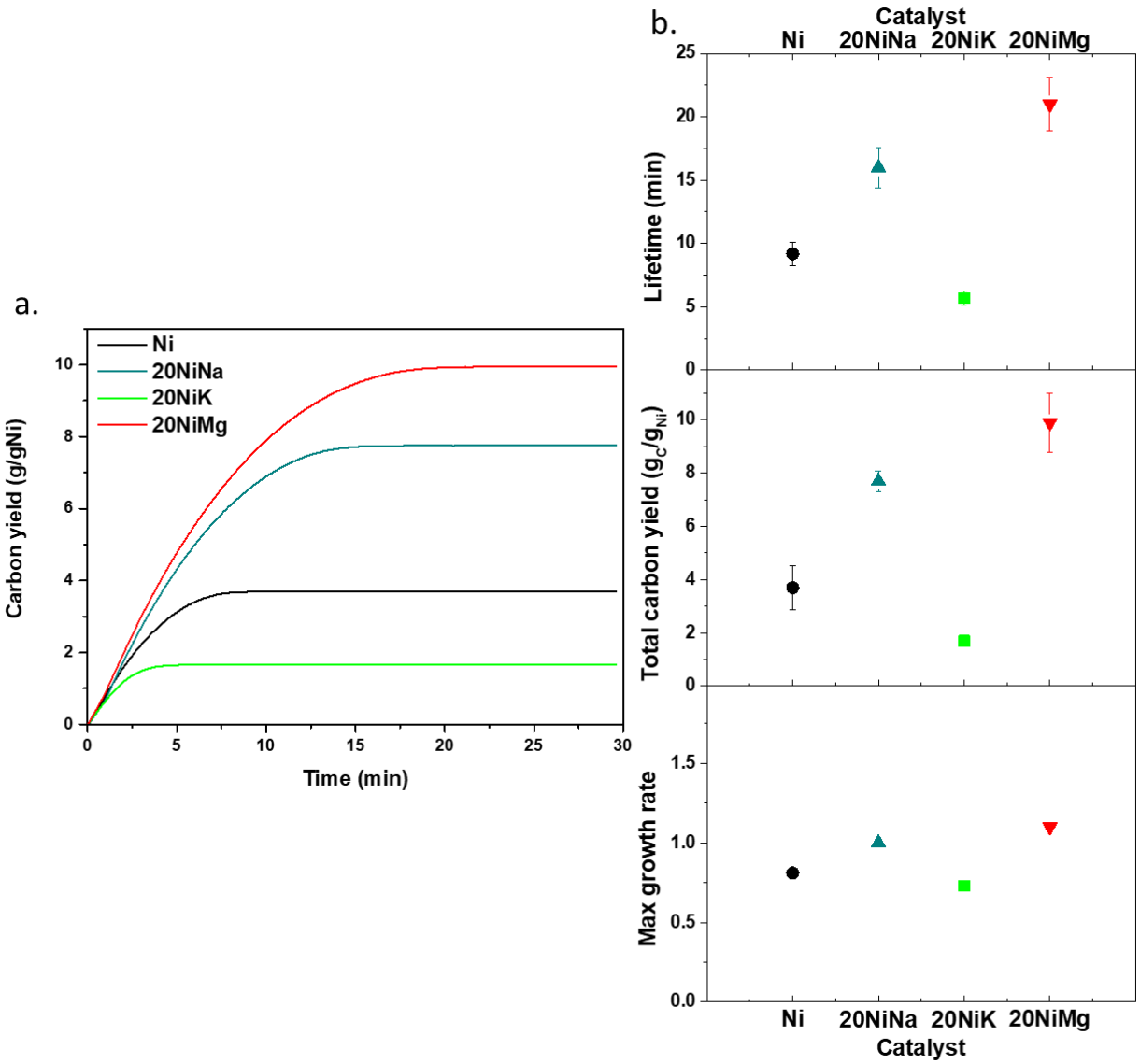

Figure 10: a. Averaged carbon yield as a function of time at 500°C in 34% CH_4/Ar for the other 20 Ni/Promoter ratio catalysts. b. Individual catalytic properties for the Ni, 20NiNa, 20NiK, and 20NiMg catalysts.

While we now know that the incorporation of the used promoters has a significant influence on the catalytic performance of the Ni catalysts, it would be very useful if this could be linked to any physical properties of the promoters. Because lifetime, total carbon yield, and max growth rates follow the same trends between the different catalysts, as shown before, the following correlations will only be shown using the lifetime. For the alkali metals electronic effects are most often seen as their primary influence, as they are said to decrease the work function of the metal surface.[34] When we take the electronegativity as a measure for these electronic effects, the electronegativity for all promoters is significantly lower than that of Ni itself. This would give all the promoters that are studied an electron-donating function within this system. When going down the row of the alkali metals we can see that the electronegativity decreases from Li to Na to K. With Mg from period 2 having the highest electronegativity of the promoters.[74] If the major role of the promotion is indeed electronic, it might be expected that a trend can be found when the catalytic data is compared to the electronegativity. The lifetime is compared to the difference in electronegativity between Ni and the promoters in Figure 11. What can be observed is that when only looking at the promoted samples, a decrease in lifetime is observed when going to lower electronegativities. However, if there would be a linear relation between the difference in electronegativity and the lifetime and activity, it would be suspected that the unpromoted catalysts would show both higher lifetime and activity. As this is not the case, the relation between ΔEM and the catalytic properties might be more parabolic in nature with an optimum around a ΔEM of -0.5, this is also shown by the dotted line in the figure.

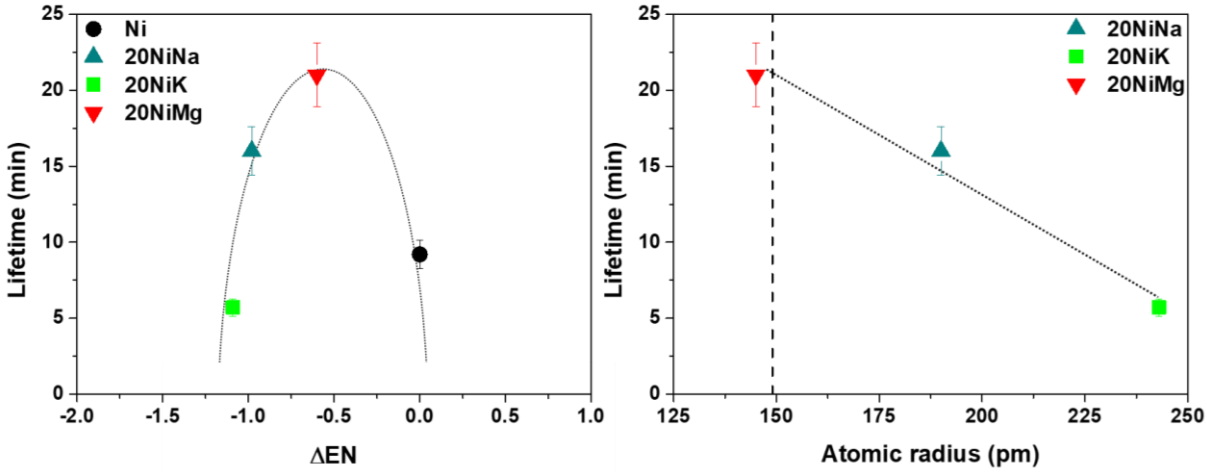

Figure 11: On the left, the dependence of the lifetime on the difference in electronegativity of the promotors to Ni, showing a parabolic dependence with a maximum around -0.5ΔEN. On the right the dependence of the promoters' atomic radii on the lifetime, showing a linear dependence with increasing lifetime upon decreasing atomic radius.

Atomic radius of the promoters, another property of the promoters beside electronegativity, might play an influential role in the difference observed in catalysis between the different catalysts as well.[75] The alkali metal promoters are expected to be present on top of the surface of the metal nanoparticles. But their presence there might be able to block certain active sites for methane dissociation, which would lead to lower reaction rates. They might also block carbon formation on the surface, resulting in slower deactivation if the carbon formation is only blocked on the part where methane is decomposed. Or it slows carbon growth if the promoters are also present at the part of the particles where the fibers are formed. On the right in Figure 11, the lifetime of the catalysts is displayed as a function of the atomic radius of the promoters. The atomic radius of Ni is displayed by the dashed line at 149 pm. From these results, the lifetime can be said to follow a linear trend as a function of the atomic radius of the promoter, with the lifetime decreasing at bigger atomic radii. This, however, can also be attributed to the concentration of the promoters in the catalysts. Because these molar concentrations are kept the

same through the different promoted catalysts, it means that the catalysts with bigger atomic radii can cover more of the Ni surface with the number of atoms present. This higher surface coverage could also have led to this linear decline of the lifetime.

While it is expected for the alkali metals to sit on the surface of the Ni particles, this might not be the case for the Mg promoter. As mentioned in the introduction, Mg can form combined phases with Ni in its metallic state, as well as in its oxidized MgO state.[57,58] This combined NiMg phase is supported by the EDX data shown previously in Figure 9. This would mean that the way Mg promotes the Ni catalysts might be significantly different than the promotion of the alkali metals, even though the trends found before seem to also apply to Mg. Mg-promotion might even have more resemblance to promotion with Cu for example, as some of Mg's physical properties are very similar to those of Cu. They have similar atomic radii, which makes it possible for both metals to form alloys with Ni. They also have similar fermi energies, which might have an influence on the solubility of carbon within Ni alloys.[33,76] These arguments might suggest that promotion with Mg gives a combination of the more geometric or structural promotional effects observed in bimetallic NiCu catalysts, with the electronic or positional effects more observed in alkali promotion.

The 20NiLi catalyst has not yet been discussed because it did not show any form of reproducibility between the different measurements done on this sample. As can be seen in Figure 12., the 20NiLi catalyst showed vastly increasing activity over the three measurements that have been performed. As the catalytic conditions were the same for all different experiments and the MS data shows no significant differences in the atmosphere during the catalytic procedure, this can not explain the large differences between these measurements. In the characterization of this catalyst, differences were already observed in both the heat treatment and the reduction characteristics of this sample in contrast to the other catalysts. Mainly, the complete oxidation back to NiO after reduction might be of influence here, as the heat treatment, while having a different TGA profile at higher temperatures, still resulted in the same NiO phase as it did for the other catalysts. Furthermore, no weight increase is observed after in situ reduction of the catalyst samples, which would indicate reoxidation by something in the gas phase. These different properties might still affect the final catalytic measurements in some way. The positioning of the Lithium ions, and their suspected counter ions, are also still unknown due to the inability to determine this using STEM-EDX or XRD. More research is needed to fully understand this Li-promoted catalytic system, nonetheless this might be worthwhile as two of the measurements show better activity than the unpromoted catalyst. Regardless of that for the remainder of this work the catalytic properties of this catalyst will not be explored further.

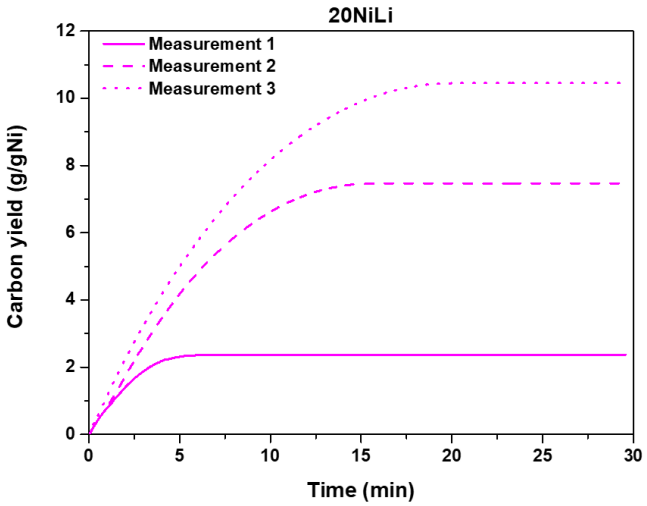

Figure 12: Carbon yield as a function of time for the three measurements performed at 500°C in 34% CH4/Ar on the 20NiLi catalyst, showing a significant increase for each measurement.

3.2.2. Varying promoter ratios

As mentioned previously, a concentration dependence might explain the trends that were found between the catalytic properties of the different promoted catalysts and the electronegativity and atomic radii, because the promoters with the most extreme properties showed lower performances than the ones with milder physical properties. This could lead to an optimization of the promotional effects at lower concentrations than were examined before. This dependence was further explored through the preparation and testing of the Na- and Mg-promoted catalysts with different molar concentrations. These measurements, which were performed at 500°C can be seen in Figure 13. In the left graph, the different NiNa concentrations are displayed, and on the right side the different NiMg catalysts. There seems to be a significant difference in the concentration dependence of these to different promoters in the tested concentration range.

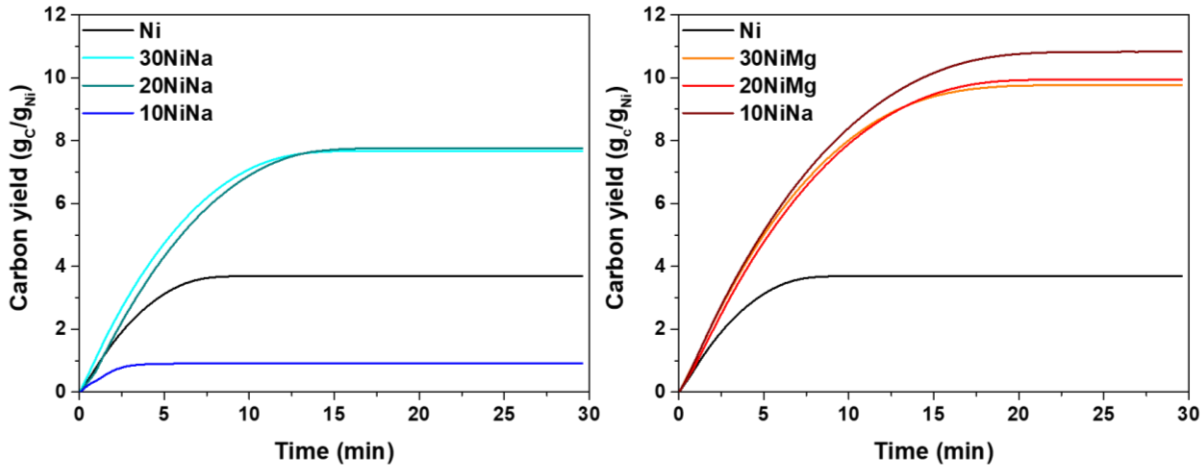

Figure 13: On the left, the carbon yield as a function of time is displayed for the Na-promoted catalysts with different promoter concentrations. On the right, the carbon yield as a function of time is displayed for the Mg-promoted catalysts with different promoter concentrations.

For the Na-promoted catalysts (Figure 13, left), it shows the 30- and 20NiNa catalysts having very similar catalytic performance, but going to a higher concentration, which means a lower atomic ratio of Ni to promoter, in the 10NiNa catalyst, the performance decreases. This would indicate that, as expected, there is a concentration dependence for these Na-promoted Ni catalysts. With the independent catalytic properties displayed on the left side of Figure 14, we can see that for the most part, the trend observed in the previous section for the different promoters is followed here as well. Longer lifetimes for the different concentrations are again accompanied by both higher total carbon yields, as well as higher maximum growth speeds. The only parameter that shows a slight difference is the max growth speed of the 20NiNa, which is slightly lower than that of the 30NiNa catalysts, while the lifetime and total carbon yield are very similar.

The Mg-promoted catalysts (Figure 13, right) show a different result than the Na-promoted catalysts. In this case, the catalytic performances show fewer differences between the different promoted catalysts. There even seems to be a slight increase when going toward higher Mg concentrations. On the right side of Figure 14, the separated parameters for the NiMg catalysts can be found. For these, as for the full catalytic TGA data, we can see that all three measurements have very similar lifetimes, carbon yields, and maximum growth rates. There is a slight increase in the carbon yield when going to higher concentrations. This, however, is not as apparent for the lifetime and the maximum growth rate. One way to interpret this data is that there is no concentration dependency for the Mg-promoted Ni catalysts, or at least not in the concentration range that we have tested here. As mentioned earlier, the

Mg- promotion is not entirely the same type of promotion as is the case for the Na-promoted catalyst. If the character of the Mg-promotion is more like the bimetallic character of NiCu catalysts, the concentrations of Mg used in the catalysts might need to be higher to have a larger effects on the catalytic performance than the concentrations that have been tested here.[77–79]

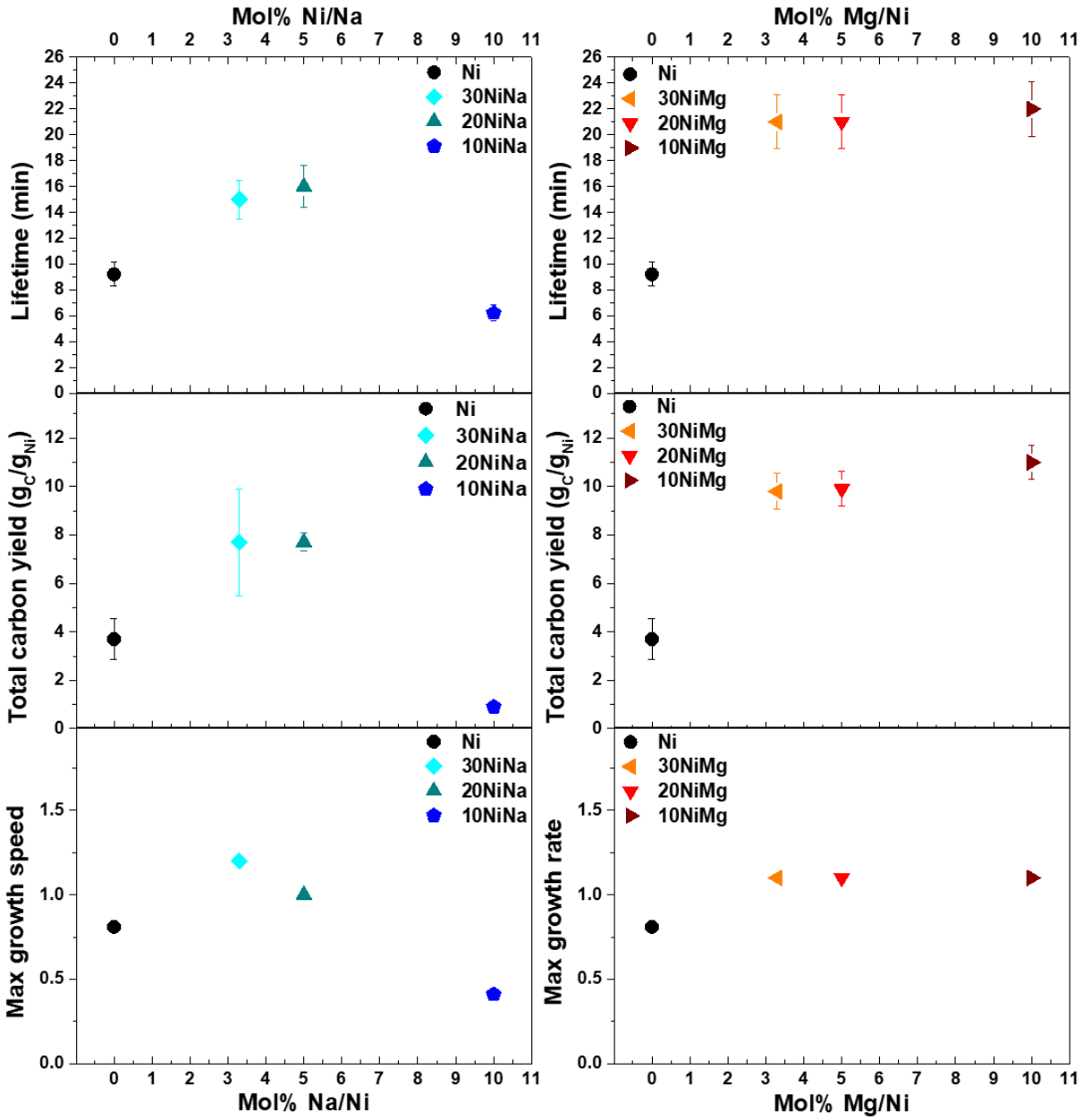

Figure 14: On the left, the different catalytic properties for the Na-promoted catalysts with different Na concentrations are shown. Showing a concentration optimum between the 30NiNa and the 20NiNa catalysts. On the right, the different catalytic properties are shown of the Mg-promoted catalysts with different concentrations. Showing a slight increase in the catalytic properties when going to higher promoter concentrations.

When looking back to the trends that were observed for the different promoters (3.2.1.), these might be explained by the concentration dependence seen for the Na-promoted catalysts. This might suggest that the low catalytic performance found for the K-promoted catalyst can be explained by a too-high concentration of K in this catalyst. As both the electronegativity as well as the atomic radius of K is more extreme than that of Na, the optimum concentration in the dependency of K might be at much lower concentrations than the one that was tested for this study. This need for lower concentrations for the

lower alkali metals would be in line with other catalysts being promoted with very small amounts of caesium for other reactions, as this has even more extreme properties than K.[80,81] It would be interesting for future research to prepare catalysts with a range of lower K concentrations to determine if this is the case, or if K is solely a poison to this reaction.

3.2.3. Temperature effect

Because of the signs that the type of promotion between the Na- and Mg-promoted catalysts is different, it would be interesting to see if they behave differently at different temperatures. To do this, the 20NiNa, 20NiMg and the reference Ni catalysts were each measured at 400, 450, and 550 °C in addition to the measurement at 500°C already shown before.

First it is important to determine if the particle sizes of the different catalysts are still comparable when the catalysts are exposed to a different temperature other than 500 °C (Table 4). The particle sizes at the lower temperatures are smaller than when catalysis was performed at higher temperatures. The only catalyst that does not follow this trend is the 20NiNa catalyst where the average particle size of the catalyst measured at 400 °C is slightly bigger than the one measured at 450 °C. Nonetheless, this difference, is well within the standard deviation in the size distribution. Because the particle sizes for the different catalysts are still very similar at the different temperatures, the catalytic results can be fairly compared. One thing to note, is that the particle sizes do increase when the temperature increases. This might influence the catalysis, but as it is similar for all catalysts, this will not influence the comparison between the catalysts.

Table 4: Average particle sizes measured using TEM images of the Ni, 20NiNa, and 20NiMg catalysts measured after in-situ reduction and heating to temperatures at which catalysis was performed.

Avg. particle size (nm)	**Ni**	**20NiNa**	**20NiMg**
400 °C	5.7 ± 1.6	7.2 ± 1.7	6.1 ± 1.5
450 °C	6.5 ± 2.1	6.5 ± 1.8	6.9 ± 1.8
500 °C	7.7 ± 2.5	8.2 ± 2.6	8.1 ± 1.9
550 °C	10 ± 4.9	10 ± 3.3	9.6 ± 3.1

The measurements at the different temperatures can be found on the left side of Figure 15. At different temperatures, very different catalytic performances can be observed. For more clarity at lower times, not the whole measurement time for the 400 °C measurement is displayed. The final lifetimes and total carbon yields for these measurements can found in the right graphs together with these parameters for the other measurements as a function of the temperature. The lifetime of the different catalysts shows a strong dependence on the temperature. At lower temperatures the lifetime is high, and it sharply decreases when going to higher temperatures. This is very similar to the lifetime dependencies on temperature that are shown in literature for other Ni-based catalysts.[82] This dependency, however, is not the same for all three catalysts that were tested. Whereas the Ni and 20NiNa catalysts show a very similar dependency with a very long lifetime of around 450 min for catalysis at 400°C followed by a very sharp decrease when performing catalysis at 450 °C, this is not followed by the 20NiMg catalyst. This catalyst shows a lower lifetime at the lowest tested temperature, but also a shallower decrease in its lifetime when going to higher temperatures.

This difference between catalysts is also found when looking at the total carbon yield at different temperatures. The Ni and 20NiNa catalyst show a somewhat linear increase in the yield when going to lower temperatures, while the 20NiMg catalyst shows a clear optimum for the carbon yield at around

450 °C. These results are quite surprising, because like the 20NiMg catalyst, literature shows optima in the total carbon yield of Ni-based catalysts within the temperature range tested here, with the optima being between 500 and 580 °C.[82,83] Meaning the optimum found for the Mg-promoted catalyst is already lower than those found in literature. This could have something to do with the incorporation of Mg into the catalyst. For the Ni and 20NiNa catalysts, it is surprising that an optimum for the carbon yield in this temperature range is not found. If only the promoted catalyst was found to not have an optimum in the total carbon yield within this temperature range, this might be ascribed to a promoter effect. However, the Ni reference catalyst also does not show an optimum, while literature suggests otherwise for other Ni-based catalysts. This might mean that this difference is found due to factors like support effects, as the catalysts used in literature, are not supported on carbon, which shows fewer support effects. Another explanation might be the setup on which the catalysis is measured, with a TGA setup being used in this work and fluidized bed reactors being used in literature.

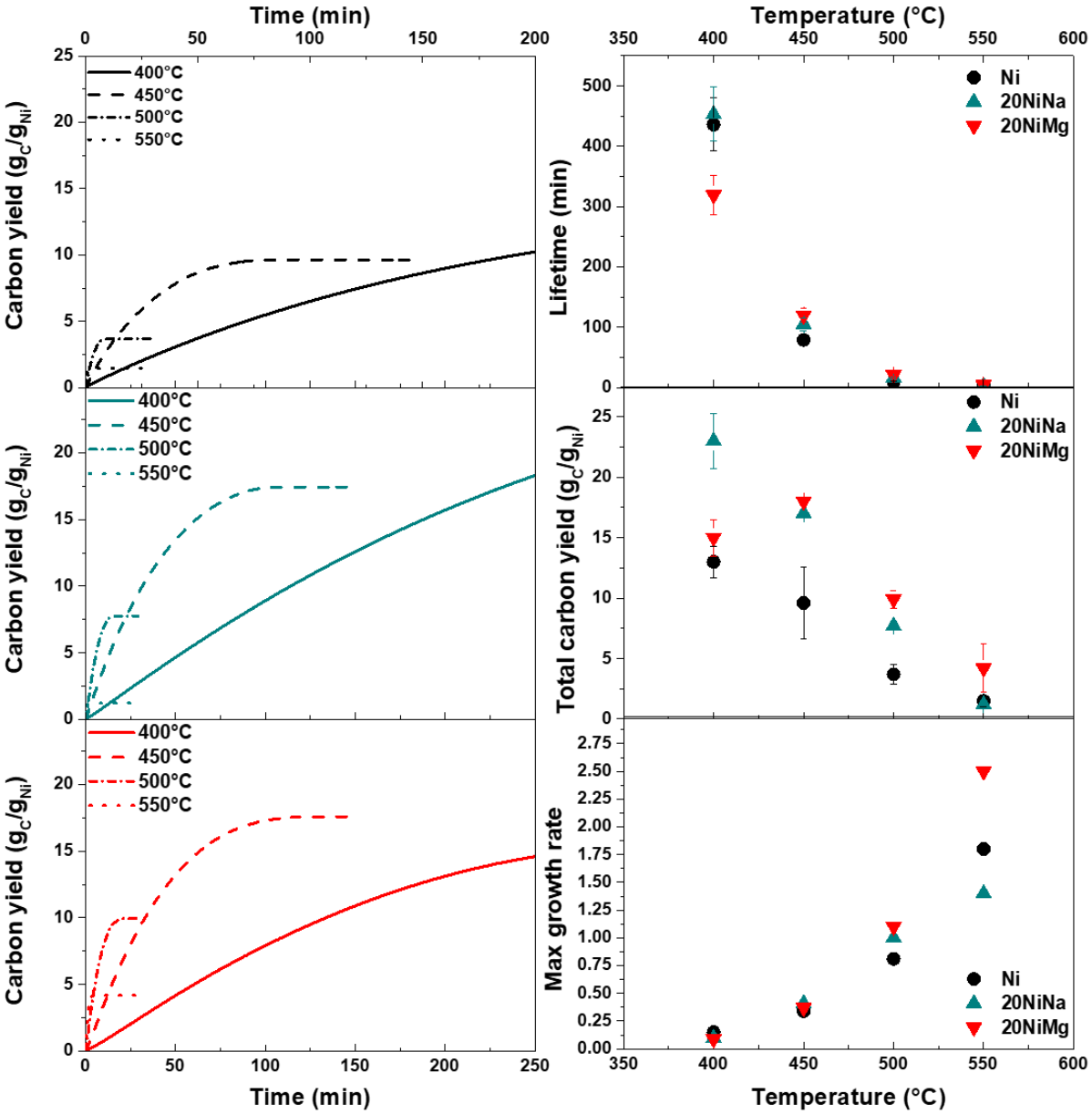

Figure 15: On the right, the carbon yield as a function of time is shown for the Ni, 20NiNa, and 20NiMg catalysts measured in 34% CH_4/Ar at different temperatures. On the right, the individual properties are shown for the Ni, 20NiNa, and 20 NiMg catalysts from the measurements on the left. Showing increasing lifetimes at lower temperatures and an optimum in total carbon yield for the 20NiMg catalyst at 450°C.

Longer lifetimes and higher total carbon yields might sound very beneficial for this reaction, this is not entirely the case because the growth rates decrease when going to lower temperatures. So while the catalysts have longer lifetimes at lower temperatures, they produce less carbon, and thus hydrogen, in a given timeframe. The most optimal situation is long lifetimes together with high growth rates. When comparing the maximum growth speeds of the different catalysts in Figure 15. We observe that unlike the lifetime, the 20NiMg catalyst shows the most extreme growth rates, whereas the other two catalysts showed the more extreme lifetimes. The higher growth rates at higher temperatures do however result in very fast decrease of these lifetimes.

When the growth rates of the three catalysts are plotted in an Arrhenius plot, the activation energies for these catalysts from the slope of the linearly fitted lines can be determined (Figure 16). The activation energy determined for the Ni reference catalysts at 77 ± 3.2 kJ/mol is in line with values found for other catalysts, where mostly activation energies between 60 and 100 kJ/mol are found.[82–87] The activation energies found for both of the promoted catalysts are higher than that of the reference catalyst, at 83 ± 13 kJ/mol for the Na-promoted sample and 102 ± 4.5 kJ/mol for the Mg-promoted catalyst. This high E_a for the Mg-promoted catalysts can explain the lower activity that was found at lower temperatures, compared to the other catalysts because not enough energy was present to overcome this energy barrier. For both the Ni and the 20NiMg, the linear line that is fitted in the Arrhenius plots is very well fitted to the measured points, which is also indicated by the low deviation in the activation energy. For the 20NiNa catalyst, however, this deviation is a lot larger as the fit of the linear line is not very good. This might be caused by experimental errors during the catalytic measurements or the presence of more than one mechanism for this reaction. As Schoemaker et al. shows for NiCu catalysts, two temperature regimes can be present as the carbon growth mechanism can change depending on the temperature.[31] Although, it is not certain that this is the case here, as too little temperatures have been measured to get a clear picture it might explain the big deviation in the fitted line.

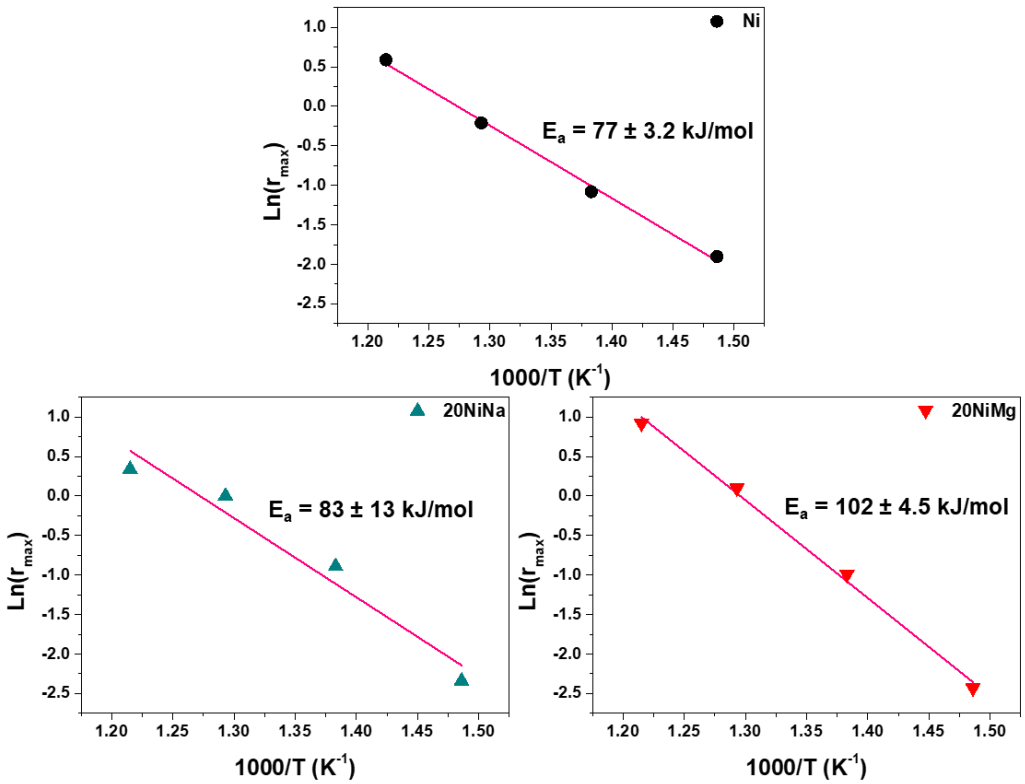

Figure 16: Arrhenius plots for the Ni, 20NiNa, and 20NiMg catalysts, with activation energies of 77 ± 3.2, 83 ± 13, and 102 ± 4.5 kJ/mol respectively.

3.2.4. Carbon product characteristics

During the catalysis, the carbon that was formed was deposited in carbon structures. Literature suggests that the carbon structures that are formed in this reaction are influenced by many different parameters, of which promotion can be one.[21] To see if the promotional effects that we researched in this work had any effect on the carbon formation, the products of one of the catalytic measurements of each catalyst and reaction condition, were imaged using TEM. From these images, the fiber diameter could be measured and the types of carbon fibers that had been grown during the reaction could be determined. For the measurements showing less activity, also fewer fibers could be measured as fewer are grown during catalysis. In this section, we will take a look at these results to determine if the promotion of Ni catalysts with alkali- and alkaline earth metals has any influence on the formed carbon structures.

The different catalysts have been tested at 500°C and the results of these measurements on the fiber diameter can be found in Table 5 together with representative TEM images of catalysts after catalysis in Figure 17. The figures with the diameter distributions of all the measurements can be found in Appendix 8. The images of the 20NiK and 20NiMg catalysts measured after catalysis at 500 °C in Figure 17 clearly show the difference of the catalytic efficiency on the amount of carbon product that is formed. The 20NiK catalysts shows verly little fibers, with the few that have been formed very close to the carbon support.whereas the 20NiMg catalyst shows a lot of fiber growth, with fibers growing hundreds of nanometers away from the support.

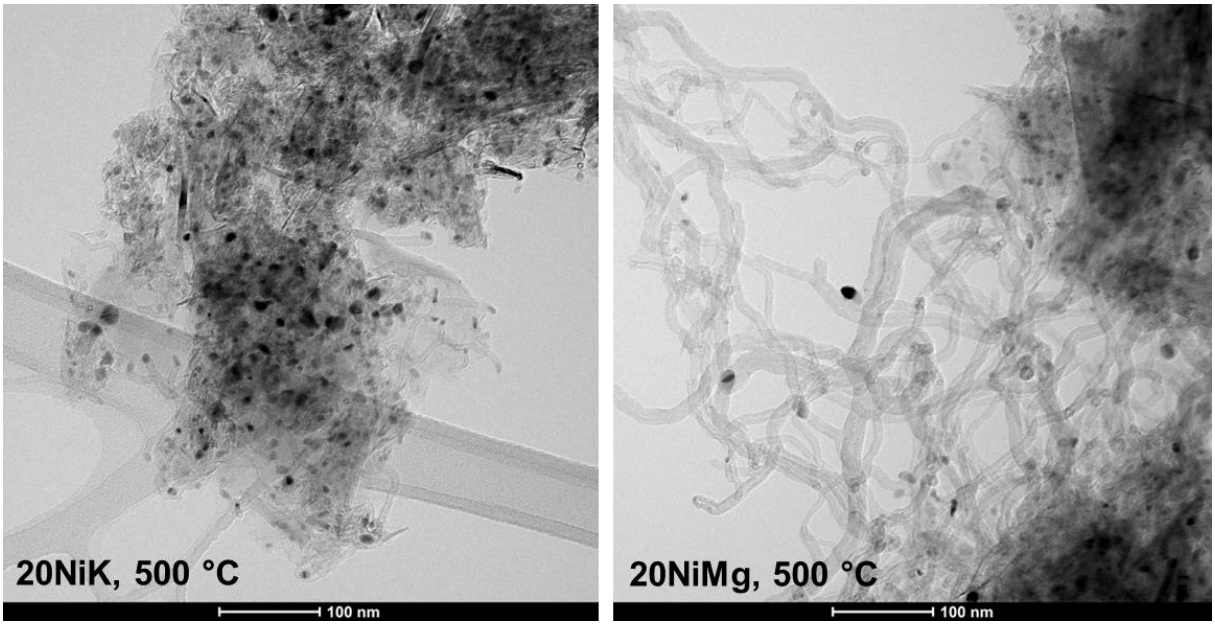

Figure 17: TEM images of catalysts 20NiK and 20NiMg after catalysis at 500 °C for 30 min in 34% CH_4/Ar with a flow of 50 mL/min.

In all images taken after the different catalytic measurements, the type of fibers that had been grown during catalysis were very similar. The predominant type of carbon structure that was formed were hollow fishbone type carbon nanofibers, as can also be seen in figure 17. While most of the fibers were hollow, some of the images also showed some full fishbone type fibers. This was observed for all the different catalysts that were measured at 500 °C. The diameters of these fibers measured for the different catalysts displayed in Table 5 are also very similar. All of the diameter distributions have a high standard deviation due to a wide distribution of the fibers observed, ranging from around 5 to 30 or 40 nm. These wide distributions in the size of the carbon fibers was also observed for all different catalysts. The only difference that seems to be present between the products of the measurements, is that when the catalysts had very low catalytic efficiencies, for the 20NiLi, 10NiNa, and 20NiK catalysts, the fiber

diameters also seem to be significantly lower than when the catalytic efficiency was higher. This can be explained by the growth of the particles during catalysis. When the catalyst particles carbon for a longer time, there is more time for the Ni particles to grow. As the particle size of the Ni nanoparticles is related to the size of fiber being grown, a very short lifetime would lead to slimmer fibers. While the catalytic efficiency is influenced by the used promoter, it does not seem that the promoters have a direct effect on the carbon nanostructures that were formed during catalysis. This could be a strong indication that the type of promotion using alkali- and alkaline earth metals does not directly effect the composition of the Ni nanoparticles or the mechanism of carbon nanofiber growth. This type of promotion might thus be more related to electronic effects or the inhibition of the growth of amorphous carbon leading to the increased lifetimes.

Table 5: Average fiber diameters of the different catalytic measurements performed at 500 °C.

	Average fiber diameter (nm)	**Standard deviation (nm)**
Ni	14.3	± 7.0
20NiLi	8.6	± 2.1
10NiNa	8.2	± 1.5
20NiNa	12.3	± 5.7
30NiNa	10.5	± 3.5
20NiK	8.3	± 2.3
10NiMg	12.9	± 3.8
20NiMg	12.4	± 4.0
30NiMg	11.9	± 3.3

For the measurements performed at different temperatures, the diameters of the formed fibers were also measured and are displayed in Table 6. At 550 °C almost no fibers had formed, so it was not possible to accurately measure any fiber diameters for these measurements. The diameters throughout the different measurements show that the sizes of the fibers are still within a very similar range, suggesting temperature does not seem to have much influence on the fiber growth. The only thing to note is that the size distributions might have broadened some in comparison to the measurements at 500 °C, which resulted in higher deviations. .

Table 6: Average fiber diameters of the Ni, 20NiNa, and 20NiMg catalysts where catalysis was performed at 400 °C, 450 °C, and 500 °C.

	Ni	**20NiNa**	**20NiMg**
400 °C	13.2 ± 3.9	15.3 ± 4.5	12.2 ± 4.1
450 °C	16.4 ± 7.0	11.8 ± 2.9	13.5 ± 4.2
500 °C	14.3 ± 7.0	12.3 ± 5.7	12.4 ± 4.0

4. Conclusions

In this work, we have attempted to gain more insight into the promotional effects of alkali and alkaline earth metals on the Ni-catalyzed thermal decomposition of methane. Different catalysts promoted with Li, Na, K, and Mg were prepared, thoroughly characterized, and tested on their catalytic properties.

The preparation of the promoted and unpromoted catalysts was performed using an incipient wetness impregnation method. Using this method, catalysts with a 20-1 Ni to promoter ratio were prepared for all different promoters. For the Na- and Mg-promoted catalysts, two extra catalysts were prepared which showed 30-1 and 10-1 Ni to promoter ratios.

Heat treatment and reduction were performed on the prepared catalysts. All different catalysts showed expected decomposition patterns during heat treatment, with only 20NiLi again having a slight difference in the autoreduction temperature. The reduction profiles for all catalysts were shown to be very similar with measured hydrogen uptakes all exceeding the theoretical uptakes needed for the reduction of NiO to Ni. This was caused by the uptake of hydrogen due to support methanation at elevated temperatures. Powder-XRD measurements were performed after both heat treatment and reduction followed by passivation. After heat treatment, all catalysts showed full decomposition of the $Ni(NO_3)_2 \bullet 6\ H_2O$ precursor to NiO. However, after reduction most of the catalyst showed metallic Ni, as well as some small NiO peaks caused by partial re-oxidation. Again, the 20NiLi catalysts yielded different resultsThis time no metallic Ni was visible in the diffractogram leading to the conclusion that the Li-promotion resulted in full oxidation of the metallic Ni phase back to the NiO phase.

The placement of the promoters on the catalysts was determined using HAADF-STEM EDX and it was shown that for both Na- and Mg-promoted catalysts the location of the promoters seemed to correspond with the Ni particles. From this, we concluded that the Na and Mg atoms are present on the catalysts for the Na-promoted catalysts, and on or in the Ni particles for the Mg-promoted catalysts.

As all catalysts had been successfully prepared and thoroughly characterized, they were all tested using a TGA-MS system for their catalytic properties in the thermal decomposition of methane. This was done to answer the following questions:

How does the promotion with Li, Na, K, and Mg of Ni/C catalysts affect the activity and lifetime of these catalysts in the thermal decomposition of methane at 500°C?

All different promoters showed significant changes in catalysis compared to the reference Ni catalysts at 500 °C, with the 20NiMg catalyst showing the highest lifetime, total carbon yield, and growth rate. In addition, the 20NiNa catalysts showed higher catalytic performances than those of the reference monometallic Ni catalyst. The only catalyst that performed worse than the reference catalysts was the 20NiK catalyst. This catalyst showed a significant reduction in catalytic activity and lifetime compared to all the other tested catalysts. As the lifetime of the catalysts was most effected upon pormotion, even though the growth rates did not change large amounts, the promotional effects might be based on the blockage of sites where amorphous carbon is deposited. Moreover, the 20NiLi catalysts showed very varying results over the three measurements that were performed, with significantly increased performance for each measurement. An explanation for these results was not found.

Is there any dependence on the concentration or temperature when promoting Ni/C with Na or Mg for the thermal decomposition of methane?

Catalysts promoted with different concentrations of Na and Mg were tested in catalysis at 500 °C to determine if any concentration dependences were present. It was shown that for the Na-promoted catalysts, an optimum could be determined in the concentration between 4 and 5 mol% Na/Ni. The

Mg-promoted catalysts did not show the same dependence on the concentration. For these catalysts, the catalytic performance seemed to slightly increase over the tested concentration range, leading us to conclude that Mg might promote the Ni-based catalysts in a different way than the alkali metals.

The dependence that was found on the temperature also differed between the Na- and Mg-promoted catalysts. It was presented that the Na-promoted catalysts showed a dependence on the temperature very similar to that found for the reference Ni catalyst, with no optimum temperature found for the lifetime and total carbon yield within the tested temperature range. However, the Mg-promoted catalyst did show an optimum of around 450°C with a more modest decline in the lifetime at lower temperatures than the other tested catalysts. This might also be an indication that the roles of the Na and Mg promoters are different in either case. Subsequently, the activation energies were reported to be 77, 83, and 102 kJ/mol for the Ni, 20NiNa, and 20NiMg catalysts respectively, which were in line with previously reported activation energies.

Can any trends be found between the promotional effects of Li, Na, K, and Mg when used to promote Ni/C catalysts for the thermal decomposition of methane?

Specific trends between the different promoters were found both based on their electronegativity difference to Ni and concerning the atomic radii of the promoter atoms. For the difference in electronegativity, an optimum was found around -0.5 ΔEN, which the 20NiMg was very close to. When increasing electronegativity differences, the catalytic performance of the catalysts was shown to rapidly decrease. For the atomic radii of the promoters, a linear relationship could be found, where the catalytic performance decreased with increasing atomic radius. This relation, however, could also be due to the concentration dependency that was found. As for both dependencies, the catalytic performance decreased for the promoters with the more extreme physical properties, which are found when going down in the alkali metal period. It might be the case that for these catalysts, positive promotional effects are only found at lower promoter concentrations, as their influence is greater.

How does the promotion with Li, Na, K, and Mg of Ni/C catalysts affect the carbon structures being formed during the thermal decomposition of methane?

Catalysis performed with the different catalysts and catalytic conditions used for this work all resulted in the formation of hollow fishbone type carbon nanofibers, with some sporadic full fibers fishbone type fibers. The different promoters that were tested did not have much influence of the growth of the fibers. This might indicate that the composition of the Ni nanoparticles is not changed much upon promotion using alkali- or alkaline earth metals, confirming the expectations that the promotional effect is based on electronic effects or the inhibition of the formation of amorphous carbon leading to deactivation of the catalysts.

With these results, more insight has been gained into the way that the alkali and alkaline earth metals promote the Ni-catalyzed thermal decomposition of methane.

5. Outlook

While we have gathered some great new insights into alkali and alkaline earth promotion for the Ni-catalyzed thermal decomposition of methane, there are still many things that can be done to improve our understanding of promotor effects. In this outlook, we will first start with looking at research that can still be done which would have a direct influence on the understanding of the results found in this work. Subsequently, we will look at different angles that can still be explored in furthering the understanding of the promotional effects of alkali and alkaline earth metals on the Ni-catalyzed CTD of methane.

The most important part to figure out related to this research would be the positioning of the promoters. As it is suspected that the presence of the promoters block sites, where amorphous carbon is formed, which leads to deactivation of the catalysts. Determining the exact promoter locations can give more insight into these suspicions. Possibilities to do this might be using XRD, from which the phases of the promoters might be determined, although higher promoter quantities might be needed. Also, more potent EDX might give more insight. Another possibility might be in computational chemistry. It might be possible to model the incorporation of the promoters on the Ni nanoparticles to determine where the promoters would end up. This might give more insight into the change in physical and electrical properties of the nanoparticles upon promotion.

Because some/several parameters that influence the catalysis directly are still unclear, gaining more insight in what they are would be very beneficial and would help in better understading the results that were found. Something that is not touched upon in this work but could have an effect on the catalysis is the counterions to the different promoters that were used. It is not expected that the promoters are present in their metallic form, as these are very sensitive to air, and would be quickly oxidized. However, it is expected that the promoters are present in their ionic form. This suggests that the negative counter ions must be present in the catalysts as well. In combination with the other components of the catalysts, the decomposition of the initial promoter salts might have been affected as well. Unfortunately the composition of the counter ions, as well as their effect on catalysis, is still very much unclear. It might be possible to shed some light on this issue by using different promoter salts in the initial precursor solution. Promoter salts with easier decomposition than the nitrate salts used in this work might make it possible to promote the Ni catalysts with metallic alkali and alkaline earth metals. When comparing these catalysts without counter ions to the catalysts used in this work, the effects of the counter ions might be cleared up.

This work also showed that the catalysts change during in-situ reduction and heating to catalytic temperatures Because of this, it might be beneficial to make sure these changes have already occurred before any catalytic testing is done. Making sure that catalysts are in a stable phase during the whole of the different catalytic measurements can reduce influences such as particle size effects when measuring catalysis at different temperatures. This might be achieved by incorporating harsher heat treatment steps within the method of catalyst synthesis. These heat treatments must be harsher than any conditions under which catalysis is performed, to form a stable catalytic phase at catalytic conditions. Hydrogen treatment at high temperatures would be the most optimal, as hydrogen is also present during the catalytic measurements. Although, the carbon support used in this study will be methanated at the elevated temperatures that would be needed, but this might need to be accepted to obtain more reproducible and comparable results.

A last possibility that could be explored to gain further understanding is measuring the catalysts in higher quantities. Performing the experiments in bigger quantities will allow us to determine if the same results are found when catalysis is scaled up. Achieving this would be impossible in the used TGA

setup, as the sample pans don't fit much more of the sample. Another catalytic setup would be needed to complete these measurements. Using a fluidized bed reactor would be the best choice as literature already discribes this would allow for free growth of the catalytic particles without much risk of breaking the catalytic setup when carbon growth occurs.[19]

Aside from more research to gain more clarity, another option is improving the understanding of the alkali and akaline earth promotion on the CTD reaction as a whole. A first logical continuation of this work being the promotion with other alkali- and alkaline earth metals like Cs, Be and Ca. It would be very insightfull to find out if these different promoters follow the trends found in this work, or if they differ from it. It is expected that Cs-promotion would follow the promotianal effects of Na, but with a much lower optimum concentration whereas the Be- and Ca-promotion would be more in line with what was found for the promotion using Mg.

For all possible promoters, differences in the catalysts might also be explored. As we have seen in this work, the promoter loadings do effect the properties of the promoted catalysts, leading us to believe that the optimization of these loadings for all the different promoters might give very interesting results and insights into how these promoters work. Another interesting property of the catalysts to explore would be if the promotional effects that have been found are effected by the support that is used for the catalysts. The metal support interactions might influence the promotional effects of the alkali- and alkaline earth metal promoters leading to different results with the use of different supports.

Finally, the differences in growth mechanism of the carbon nanostructures can be explored upon addition of the promoters. One suggested method of doing this would be to follow the growth of the carbon using in-situ TEM. This method would allow for visualization of both the nucleation of the carbon structures aswell as the more continuous growth stage once the structures are growing. In turn, this data might be used to shed more light on any changes in the growth mechanisms of the carbon nanostructures between the promoted and unpromoted catalysts.

Apart from giving more insight into promotional effects in general, all these mentioned avenues of research might help us gain better understanding of the alkali- and alkaline earth metal promotion in the Ni catalyzed thermal decomposition of methane.

6. Acknowledgements

To be able to perform all the research done in this work, many parties have made important contributions. Therefore, I would like to thank various people for all the help thay gave me during this project. Without them this work would not have been possible.

First and foremost, Suzan Schoemaker, not only for being my daily supervisor during the project, but also for being someone who was great to talk to, work with, and made me feel right at home in the group.

I would also like to thank my examiners, Prof. Petra de Jongh and Dr. Jessi van der Hoeven, apart from just examining me and making the project possible, they also provided great feedback and discussion along the way.

Hans and Tom, who were essential in all the work that they did for this project on the microscope, making beautiful images of both the catalysts before and after catalysis. Without these images, a large part of the project would not have happened.

Nienke en Kris, I would like to thank for all the help, supervising me when Suzan wasn't available and the great in-depth discussions that we had on my topic, sometimes it really led to a little breakthrough!

The technicians, mainly Dennie with his help with the TGA, were really invaluable. Without their hard work, none of this would have been possible.

The rest of the group, including the master students, was always there for a nice cup of coffee or a distracting talk whenever needed. A very inviting atmosphere with a lot of fun activities. They all give a warm welcome to anyone that comes into the group. They all made it an amazing experience.

Aside from the group, some people in my personal life have made a great contribution. Sometimes to vent about the project or the day, and sometimes just to talk to and work through some problems we were facing during the thesis.

So for all of the people mentioned above, you made this previous year working on my thesis at MCC a very memorable and great experience, it will not soon be forgotten. So for that, thank you, and maybe I'll be back :D.

7. Layman's abstract

The current way of producing the bulk of our energy cause large amounts of emissions, which lead to climate change. Although, green methods of producing energy, like wind or solar energy are being developed, these methods are not yet ready to meet the rising energy demands. An intermediate solution might be to use the current resources, like methane gas, in an emission-free way. When methane is heated without the presence of air, it falls apart into H_2 gas and solid carbon, instead of harmful CO_2. In turn, the H_2 gas can be burned in conventional ways to produce energy without the emission of any harmful gasses. The solid carbon that is formed during this reaction also has added value as it can be used in multiple applications.

The process to split methane into carbon and hydrogen is called thermal decomposition. For this reaction to take place, very high temperatures are needed. It takes large amounts of energy to achieve these high energies, which is undesirable. To lower the required energy that is needed for the reaction to take place, catalysts are used. There are many possible catalysts that can be used for this reaction,

but in this work, we focus on the use of very small nickel particles, which have been put on an inert carbon material. This carbon acts as a support for the particles, keeping them stable. While these Ni particles already increase the energy efficiency of the reaction on their own, it is still possible to improve on this efficiency by tuning the properties of the Ni particles. There are multiple ways to achieve this, but we will focus on the improvement by the addition of very small amounts of a different element, which is called promotion. The addition of the different elements from the periodic table will result in different effects on the catalysts. The focus of this work will be on the addition of Lithium (Li), Sodium (Na), Potassium (K), and Magnesium (Mg) as promotors which are elements from period 1 and 2 of the periodic table. These used elements are suspected to influence the electronic or surface properties of the Ni particles the most, thus inducing great changes in the catalytic efficiency.

By preparing catalysts in which the different promoters were incorporated it was found that only the Na- and Mg-promoted catalysts improved the efficiency of the reaction. The promotion with Li did show differences with the catalysts using no promotor, however, the measurements could not be reproduced, so Li-promotion was not investigated further. Only the addition of K made the catalysts work much worse compared to catalysts using no promotor.

Because very small amounts of promoter can lead to very large effects in the thermal decomposition, the amount of promoter used also plays an important role. This is why, for the Na- and Mg-promoted catalysts, different amounts of promoter were also tested. An optimum amount of Na promoter was found. However, for Mg it was found that the efficiency slightly increased when more Mg was added. This difference gave an indication that the elements of period 1 might promote the catalyst differently than those of group 2.

The temperature at which thermal decomposition is performed is also very important, as it can give us more insight into how the promotion works. Both the Na- and Mg-promoted catalysts were tested at different reaction temperatures and compared to unpromoted catalysts. The results showed that for the Mg-promoted catalyst an optimal temperature for the catalytic efficiency was found. However, the Na- and unpromoted catalysts, worked better at the lower tested temperature. This provides another hint that the Na- and Mg-promoters work in different ways.

As mentioned before, thermal decomposition not only produces H_2 but also solid carbon. This carbon is made into different structures which have different properties. Which carbon structures are formed can be influenced by the catalyst used in the reaction. However, the addition of the different promoters did not change the structure of the produced carbon in a significant way.

All these results gave us some more insight into how the use of Lithium, Sodium, Potassium, and Magnesium can play a role as promoters in the thermal decomposition of methane, whether they improved the catalytic performance, or made it much worse.

8. Bibliography

(1) CO2 emissions - Our World in Data https://ourworldindata.org/co2-emissions (accessed Apr 10, 2023).

(2) CO2 Emissions in 2022 – Analysis - IEA https://www.iea.org/reports/co2-emissions-in-2022 (accessed Apr 10, 2023).

(3) Emissions by sector - Our World in Data https://ourworldindata.org/emissions-by-sector (accessed Apr 10, 2023).

(4) Chemicals – Analysis - IEA https://www.iea.org/reports/chemicals (accessed Apr 10, 2023).

(5) The 4th Generation - Life Cycle Emissions of Hydrogen https://4thgeneration.energy/life-cycles-emissions-of-hydrogen/ (accessed Apr 15, 2022).

(6) Bhat, S. A.; Sadhukhan, J. Process Intensification Aspects for Steam Methane Reforming: An Overview. *AIChE J.* **2009**, *55* (2), 408–422. https://doi.org/10.1002/AIC.11687.

(7) Muradov, N. Z. How to Produce Hydrogen from Fossil Fuels without CO2 Emission. *Int. J. Hydrogen Energy* **1993**, *18* (3), 211–215. https://doi.org/10.1016/0360-3199(93)90021-2.

(8) New technologies https://www.basf.com/global/en/who-we-are/sustainability/we-produce-safely-and-efficiently/energy-and-climate-protection/carbon-management/innovations-for-a-climate-friendly-chemical-production.html#text-1002215085 (accessed May 15, 2023).

(9) De Jong, K. P.; Geus, J. W. Carbon Nanofibers: Catalytic Synthesis and Applications. *http://dx.doi.org/10.1081/CR-100101954* **2007**, *42* (4), 481–510. https://doi.org/10.1081/CR-100101954.

(10) Georgakilas, V.; Perman, J. A.; Tucek, J.; Zboril, R. Broad Family of Carbon Nanoallotropes: Classification, Chemistry, and Applications of Fullerenes, Carbon Dots, Nanotubes, Graphene, Nanodiamonds, and Combined Superstructures. *Chem. Rev.* **2015**, *115* (11), 4744–4822. https://doi.org/10.1021/CR500304F/ASSET/IMAGES/CR500304F.SOCIAL.JPEG_V03.

(11) Henao, W.; Cazaña, F.; Tarifa, P.; Romeo, E.; Latorre, N.; Sebastian, V.; Delgado, J. J.; Monzón, A. Selective Synthesis of Carbon Nanotubes by Catalytic Decomposition of Methane Using Co-Cu/Cellulose Derived Carbon Catalysts: A Comprehensive Kinetic Study. **2020**. https://doi.org/10.1016/j.cej.2020.126103.

(12) Pinilla, J. L.; Moliner, R.; Suelves, I.; Lázaro, M. J.; Echegoyen, Y.; Palacios, J. M. Production of Hydrogen and Carbon Nanofibers by Thermal Decomposition of Methane Using Metal Catalysts in a Fluidized Bed Reactor. *Int. J. Hydrogen Energy* **2007**, *32*, 4821–4829. https://doi.org/10.1016/j.ijhydene.2007.08.013.

(13) Yadav, D.; Amini, F.; Ehrmann, A. Recent Advances in Carbon Nanofibers and Their Applications-A Review. **2020**. https://doi.org/10.1016/j.eurpolymj.2020.109963.

(14) Serp, P.; Corrias, M.; Kalck, P. Carbon Nanotubes and Nanofibers in Catalysis. *Appl. Catal. A Gen.* **2003**, *253* (2), 337–358. https://doi.org/10.1016/S0926-860X(03)00549-0.

(15) Krans, N. A.; Van Der Feltz, E. C.; Ie, J.; Dugulan, I. A.; Ečevicečevic´, [a], J.; De Jong, K. P. Attachment of Iron Oxide Nanoparticles to Carbon Nanotubes and the Consequences for Catalysis. https://doi.org/10.1002/cctc.201800487.

(16) Mestl, G.; Maksimova, N. I.; Keller, N.; Roddatis, V. V; Schlögl, R. Carbon Nanofilaments in Heterogeneous Catalysis: An Industrial Application for New Carbon Materials?**. *Angew. Chem. Int. Ed* **2001**, *40* (11). https://doi.org/10.1002/1521-3773(20010601)40:11<2066::AID-ANIE2066>3.0.CO;2-I.

(17) Muradov, N. Catalysis of Methane Decomposition over Elemental Carbon.

(18) Bayat, N.; Meshkani, F.; Rezaei, M. Thermocatalytic Decomposition of Methane to COx-Free Hydrogen and Carbon over Ni–Fe–Cu/Al2O3 Catalysts. *Int. J. Hydrogen Energy* **2016**, *41* (30), 13039–13049. https://doi.org/10.1016/J.IJHYDENE.2016.05.230.

(19) Amin, A. M.; Croiset, E.; Epling, W. Review of Methane Catalytic Cracking for Hydrogen Production. *Int. J. Hydrogen Energy* **2011**, *36* (4), 2904–2935. https://doi.org/10.1016/J.IJHYDENE.2010.11.035.

(20) Avdeeva, L. B.; Reshetenko, T. V.; Ismagilov, Z. R.; Likholobov, V. A. Iron-Containing Catalysts of Methane Decomposition: Accumulation of Filamentous Carbon. *Appl. Catal. A Gen.* **2002**, *228* (1–2), 53–63. https://doi.org/10.1016/S0926-860X(01)00959-0.

(21) Dupuis, A. C. The Catalyst in the CCVD of Carbon Nanotubes—a Review. *Prog. Mater. Sci.* **2005**, *50* (8), 929–961. https://doi.org/10.1016/J.PMATSCI.2005.04.003.

(22) Dai, H. Carbon Nanotubes: Opportunities and Challenges.

(23) Cassell, A. M.; Raymakers, J. A.; Kong, J.; Dai, H. Large Scale CVD Synthesis of Single-Walled Carbon Nanotubes. *J. Phys. Chem. B* **1999**, *103* (31), 6484–6492. https://doi.org/10.1021/JP990957S/ASSET/IMAGES/LARGE/JP990957SF00011.JPEG.

(24) Syed Muhammad, A. F. ad; Awad, A.; Saidur, R.; Masiran, N.; Salam, A.; Abdullah, B. Recent Advances in Cleaner Hydrogen Productions via Thermo-Catalytic Decomposition of Methane: Admixture with Hydrocarbon. *Int. J. Hydrogen Energy* **2018**, *43* (41), 18713–18734. https://doi.org/10.1016/J.IJHYDENE.2018.08.091.

(25) Bayat, N.; Rezaei, M.; Meshkani, F. Methane Dissociation to COx-Free Hydrogen and Carbon Nanofiber over Ni-Cu/Al2O3 Catalysts. *Fuel* **2017**, *195*, 88–96. https://doi.org/10.1016/j.fuel.2017.01.039.

(26) Karimi, S.; Bibak, F.; Meshkani, F.; Rastegarpanah, A.; Deng, J.; Liu, Y.; Dai, H. Promotional Roles of Second Metals in Catalyzing Methane Decomposition over the Ni-Based Catalysts for Hydrogen Production: A Critical Review. *Int. J. Hydrogen Energy* **2021**, *46* (39), 20435–20480. https://doi.org/10.1016/J.IJHYDENE.2021.03.160.

(27) Wang, W.; Wang, H.; Yang, Y.; Jiang, S. Ni-SiO 2 and Ni-Fe-SiO 2 Catalysts for Methane Decomposition to Prepare Hydrogen and Carbon Filaments. *Int. J. Hydrogen Energy* **2012**, *37* (11), 9058–9066. https://doi.org/10.1016/J.IJHYDENE.2012.03.003.

(28) Wang, Y.; Zhang, Y.; Zhao, S.; Zhu, J.; Jin, L.; Hu, H. Preparation of Bimetallic Catalysts Ni-Co and Ni-Fe Supported on Activated Carbon for Methane Decomposition. *Carbon Resour. Convers.* **2020**, *3*, 190–197. https://doi.org/10.1016/J.CRCON.2020.12.002.

(29) Bayat, N.; Rezaei, M.; Meshkani, F. Methane Decomposition over Ni–Fe/Al2O3 Catalysts for Production of COx-Free Hydrogen and Carbon Nanofiber. *Int. J. Hydrogen Energy* **2016**, *41* (3), 1574–1584. https://doi.org/10.1016/J.IJHYDENE.2015.10.053.

(30) Takenaka, S.; Shigeta, Y.; Tanabe, E.; Otsuka, K. Methane Decomposition into Hydrogen and Carbon Nanofibers over Supported Pd–Ni Catalysts. *J. Catal.* **2003**, *220* (2), 468–477. https://doi.org/10.1016/S0021-9517(03)00244-6.

(31) Schoemaker, S. E.; Welling, T. A. J.; Wezendonk, D. F. L.; Reesink, B. H.; van Bavel, A. P.; de Jongh, P. E. Carbon Nanofiber Growth from Methane over Carbon-Supported NiCu Catalysts: Two Temperature Regimes. *Catal. Today* **2023**, *418*, 114110. https://doi.org/10.1016/J.CATTOD.2023.114110.

(32) Shen, Y.; Lua, A. C. Synthesis of Ni and Ni–Cu Supported on Carbon Nanotubes for Hydrogen and Carbon Production by Catalytic Decomposition of Methane. *Appl. Catal. B Environ.* **2015**, *164*, 61–69. https://doi.org/10.1016/J.APCATB.2014.08.038.

(33) Nicholson, M. E. The Solubility of Carbon in Nickel-Copper Alloys at 1000 C. *FIZ Tverd TELA* **1962**, *224* (3), 533–535.

(34) Błaszczyszyn, R.; Błaszczyszyn, M.; Męclewski, R. Work Function of the Adsorption System of Potassium on Tungsten. *Surf. Sci.* **1975**, *51* (2), 396–408. https://doi.org/10.1016/0039-6028(75)90390-8.

(35) Koel, B. E.; Kim, J. *"Promoters and Poisons." Handbook of Heterogeneous Catalysis*; Elsevier, 1987; Vol. 14.

(36) Hutchings, G. J. Promotion in Heterogeneous Catalysis: A Topic Requiring a New Approach? *Catal. Lett. 2001 751* **2001**, *75* (1), 1–12. https://doi.org/10.1023/A:1016784122682.

(37) Wilk, B.; Pelka, R.; Arabczyk, W. Study of the Iron Catalyst for Ammonia Synthesis by Chemical Potential Programmed Reaction Method. **2017**. https://doi.org/10.1021/acs.jpcc.6b09607.

(38) Torres Galvis, H. M.; Koeken, A. C. J.; Bitter, J. H.; Davidian, T.; Ruitenbeek, M.; Dugulan, A. I.; De Jong, K. P. Effects of Sodium and Sulfur on Catalytic Performance of Supported Iron Catalysts for the Fischer–Tropsch Synthesis of Lower Olefins. *J. Catal.* **2013**, *303*, 22–30. https://doi.org/10.1016/J.JCAT.2013.03.010.

(39) Borowiecki, T.; Denis, A.; Rawski, M.; Gołębiowski, A.; Stołecki, K.; Dmytrzyk, J.; Kotarba, A. Studies of Potassium-Promoted Nickel Catalysts for Methane Steam Reforming: Effect of Surface Potassium Location. *Appl. Surf. Sci.* **2014**, *300*, 191–200. https://doi.org/10.1016/J.APSUSC.2014.02.053.

(40) Ghods, B.; Meshkani, F.; Rezaei, M. Effects of Alkaline Earth Promoters on the Catalytic Performance of the Nickel Catalysts Supported on High Surface Area Mesoporous Magnesium Silicate in Dry Reforming Reaction. *Int. J. Hydrogen Energy* **2016**, *41* (48), 22913–22921. https://doi.org/10.1016/J.IJHYDENE.2016.10.020.

(41) Sutthiumporn, K.; Kawi, S. Promotional Effect of Alkaline Earth over NieLa 2 O 3 Catalyst for CO 2 Reforming of CH 4 : Role of Surface Oxygen Species on H 2 Production and Carbon Suppression. **2011**. https://doi.org/10.1016/j.ijhydene.2011.08.022.

(42) Pompeo, F.; Nichio, N. N.; González, G.; Montes, M. Characterization of Ni/SiO 2 and Ni/Li-SiO 2 Catalysts for Methane Dry Reforming. **2005**. https://doi.org/10.1016/j.cattod.2005.07.024.

(43) Franz, R.; Franz, R.; Kühlewind, T.; Shterk, G.; Abou-Hamad, E.; Parastaev, A.; Uslamin, E.; Hensen, E. J. M.; Kapteijn, F.; Gascon, J.; Pidko, E. A. Impact of Small Promoter Amounts on Coke Structure in Dry Reforming of Methane over Ni/ZrO 2. *Catal. Sci. Technol.* **2020**, *10* (12), 3965–3974. https://doi.org/10.1039/D0CY00817F.

(44) Hussain, T.; Mazhar, M.; Iqbal, S.; Gul, S.; Hussain, M.; Larachi, F. Production of Hydrogen and Carbon Nanotubes from Catalytic Decomposition of Methane over Ni:Cu/Alumina Modified Supported Catalysts. *Carbon Nanotub. Bull. Korean Chem. Soc* **2007**, *28* (7).

(45) Hussain, S. T.; Gul, S.; Mazhar, M.; Anjum, D. H.; Larachi, F. Effect of Surface Structure on the Catalytic Behavior of Ni:Cu/Al and Ni:Cu:K/Al Catalysts for Methane Decomposition. *J. Nat. Gas Chem.* **2008**, *17* (4), 374–382. https://doi.org/10.1016/S1003-9953(09)60012-8.

(46) Zapata, B.; Valenzuela, M. A.; Palacios, J.; Torres-Garcia, E. Effect of Ca, Ce or K Oxide Addition on the Activity of Ni/SiO2 Catalysts for the Methane Decomposition Reaction. *Int. J. Hydrogen Energy* **2010**, *35* (21), 12091–12097. https://doi.org/10.1016/J.IJHYDENE.2009.09.072.

(47) Musamali, R.; Isa, Y. M. A Novel Catalyst System for Methane Decomposition. *Int. J. Energy Res.* **2018**, *42* (14), 4372–4382. https://doi.org/10.1002/ER.4175.

(48) Qian, W.; Liu, T.; Wei, F.; Wang, Z.; Wang, D.; Li, Y. Carbon Nanotubes with Large Cores Produced by Adding Sodium Carbonate to the Catalyst. *Carbon N. Y.* **2003**, *41* (13), 2683–2686. https://doi.org/10.1016/S0008-6223(03)00382-8.

(49) Takenaka, S.; Ishida, M.; Serizawa, M.; Tanabe, E.; Otsuka, K. Formation of Carbon Nanofibers and Carbon Nanotubes through Methane Decomposition over Supported Cobalt Catalysts. *J. Phys. Chem. B* **2004**, *108* (31), 11464–11472. https://doi.org/10.1021/JP048827T.

(50) Takenaka, S.; Ogihara, H.; Yamanaka, I.; Otsuka, K. Decomposition of Methane over Supported-Ni Catalysts: Effects of the Supports on the Catalytic Lifetime. *Appl. Catal. A Gen.* **2001**, *217*, 101–110.

(51) Ermakova, M. A.; Ermakov, D. Y.; Kuvshinov, G. G.; Plyasova, L. M. New Nickel Catalysts for the Formation of Filamentous Carbon in the Reaction of Methane Decomposition. *J. Catal.* **1999**, *187* (1), 77–84. https://doi.org/10.1006/JCAT.1999.2562.

(52) Visser, N. L.; Daoura, O.; Plessow, P. N.; Smulders, L. C. J.; de Rijk, J. W.; Stewart, J. A.; Vandegehuchte, B. D.; Studt, F.; van der Hoeven, J. E. S.; de Jongh, P. E. Particle Size Effects of Carbon Supported Nickel Nanoparticles for High Pressure CO2 Methanation. *ChemCatChem* **2022**, *14* (22). https://doi.org/10.1002/CCTC.202200665.

(53) Dalebout, R.; Barberis, L.; Visser, N. L.; van der Hoeven, J. E. S.; van der Eerden, A. M. J.; Stewart, J. A.; Meirer, F.; de Jong, K. P.; de Jongh, P. E. Manganese Oxide as a Promoter for Copper Catalysts in CO2 and CO Hydrogenation. *ChemCatChem* **2022**, *14* (19), e202200451. https://doi.org/10.1002/CCTC.202200451.

(54) Dalebout, R.; Barberis, L.; Totarella, G.; Turner, S. J.; La Fontaine, C.; De Groot, F. M. F.; Carrier, X.; Van Der Eerden, A. M. J.; Meirer, F.; De Jongh, P. E. Insight into the Nature of the ZnOx Promoter during Methanol Synthesis. *ACS Catal.* **2022**, *12* (11), 6628–6639. https://doi.org/10.1021/ACSCATAL.1C05101/ASSET/IMAGES/LARGE/CS1C05101_0009.JPEG.

(55) Brockner, W.; Ehrhardt, C.; Gjikaj, M. Thermal Decomposition of Nickel Nitrate Hexahydrate, Ni(NO3)2·6H2O, in Comparison to Co(NO3)2·6H2O and Ca(NO3)2·4H2O. *Thermochim. Acta* **2007**, *456* (1), 64–68. https://doi.org/10.1016/J.TCA.2007.01.031.

(56) Ermakova, M. A.; Ermakov, D. Y.; Kuvshinov, G. G.; Plyasova, L. M. New Nickel Catalysts for the Formation of Filamentous Carbon in the Reaction of Methane Decomposition. *J. Catal.* **1999**, *187* (1), 77–84. https://doi.org/10.1006/JCAT.1999.2562.

(57) Zinkevich, M.; Geupel, S.; Aldinger, F. Thermodynamic Assessment of the Ternary Systems Ga-Mg-O, Ga-Ni-O, Mg-Ni-O and Extrapolation to the Ga-Mg-Ni-O Phase Diagram. *J. Alloys Compd.* **2005**, *393*, 154–166. https://doi.org/10.1016/j.jallcom.2004.09.069.

(58) Jacob, M. H. G.; Spencerb, P. J.; Rir, L. A CRITICAL THERMODYNAMIC EVALUATION OF THE SYSTEM MG-NI. **1998**, *22* (4), 513–525.

(59) Rayner-Canham, G. Isodiagonality in the Periodic Table. https://doi.org/10.1007/s10698-011-9108-y.

(60) Savitzky, A.; Golay, M. J. E. Smoothing and Differentiation of Data by Simplified Least Squares Procedures. *Anal.*

Chem. **1964**, *36* (8), 1627–1639. https://doi.org/10.1021/AC60214A047/ASSET/AC60214A047.FP.PNG_V03.

(61) Xiong, H.; Moyo, M.; Rayner, M. K.; Jewell, L. L.; Billing, D. G.; Coville, N. J. Autoreduction and Catalytic Performance of a Cobalt Fischer-Tropsch Synthesis Catalyst Supported on Nitrogen-Doped Carbon Spheres. https://doi.org/10.1002/cctc.200900309.

(62) Kust, R. N.; Burke, J. D. Thermal Decomposition in Alkali Metal Nitrate Melts. *Inorg. Nucl. Chem. Lett.* **1970**, *6* (3), 333–335. https://doi.org/10.1016/0020-1650(70)80243-4.

(63) Ruiz, M. L.; Lick, I. D.; Ponzi, M. I.; Castellón, E. R.; Jiménez-López, A.; Ponzi, E. N. Thermal Decomposition of Supported Lithium Nitrate Catalysts. *Thermochim. Acta* **2010**, *499* (1–2), 21–26. https://doi.org/10.1016/J.TCA.2009.10.016.

(64) Zhang, M.-H.; Chen, X.; Dong, H. A Study on Multistep Thermal Decomposition Behavior and Kinetics of Magnesium Nitrate Hydrate. **2021**. https://doi.org/10.1016/j.tca.2021.178951.

(65) Madarász, J.; Varga, P.; Pokol, G. Evolved Gas Analyses (TG/DTA-MS and TG-FTIR) on Dehydration and Pyrolysis of Magnesium Nitrate Hexahydrate in Air and Nitrogen. **2006**. https://doi.org/10.1016/j.jaap.2006.12.024.

(66) Bitter, J. H.; Van Der Lee, M. K.; Slotboom, A. G. T.; Van Dillen, A. J.; De Jong, K. P. Synthesis of Highly Loaded Highly Dispersed Nickel on Carbon Nanofibers by Homogeneous Deposition-Precipitation.

(67) Daoura, O.; Fornasieri, G.; Boutros, M.; El Hassan, N.; Beaunier, P.; Thomas, C.; Selmane, M.; Miche, A.; Sassoye, C.; Ersen, O.; Baaziz, W.; Massiani, P.; Bleuzen, A.; Launay, F. One-Pot Prepared Mesoporous Silica SBA-15-like Monoliths with Embedded Ni Particles as Selective and Stable Catalysts for Methane Dry Reforming. *Appl. Catal. B Environ.* **2021**, *280*, 119417. https://doi.org/10.1016/J.APCATB.2020.119417.

(68) Ashik, U. P. M.; Wan Daud, W. M. A.; Abbas, H. F. Production of Greenhouse Gas Free Hydrogen by Thermocatalytic Decomposition of Methane – A Review. *Renew. Sustain. Energy Rev.* **2015**, *44*, 221–256. https://doi.org/10.1016/J.RSER.2014.12.025.

(69) Díaz, A.; Acosta, D. R.; Odriozola, J. A.; Montes, M. Characterization of Alkali-Doped Ni/SiO 2 Catalysts. **1997**.

(70) Arena, F.; Chuvilin, A. L.; Parmaliana, A. Characterization of Li-Doped Ni/MgO Catalysts. *J. Phys. Chem* **1995**, *99*.

(71) Xu, M.; Lopez-Ruiz, J. A.; Kovarik, L.; Bowden, M. E.; Davidson, S. D.; Weber, R. S.; Wang, I.-W.; Hu, J.; Dagle, R. A. Structure Sensitivity and Its Effect on Methane Turnover and Carbon Co-Product Selectivity in Thermocatalytic Decomposition of Methane over Supported Ni Catalysts. **2020**. https://doi.org/10.1016/j.apcata.2020.117967.

(72) Li, Y.; Lu, Y.; Adelhelm, P.; Titirici, M.-M.; Hu, Y.-S. Intercalation Chemistry of Graphite: Alkali Metal Ions and Beyond. *Chem. Soc. Rev* **2019**, *48*, 4655. https://doi.org/10.1039/c9cs00162j.

(73) Zheng, T.; Reimers, J. N.; Dahn, J. R. Effect of Turbostratic Disorder in Graphitic Carbon Hosts on the Intercalation of Lithium. *Phys. Rev. B* **1995**, *51* (2), 734. https://doi.org/10.1103/PhysRevB.51.734.

(74) Allred, A. L. ELECTRONEGATIVITY VALUES FROM THERMOCHEMICAL DATA. *Nucl. Chem* **1961**, *17*, 215.

(75) Slater, J. C. Atomic Radii in Crystals. *J. Chem. Phys.* **2004**, *41* (10), 3199. https://doi.org/10.1063/1.1725697.

(76) Ashcroft, N. W.; Mermin, N. D. *Solid State Physics.*; Saunders college,: Philadelphia, Pa. :, 1976.

(77) Shen, Y.; Chong Lua, A. Synthesis of Ni and Ni-Cu Supported on Carbon Nanotubes for Hydrogen and Carbon Production by Catalytic Decomposition of Methane. *Appl. Catal. B Environ.* **2015**, *164*, 61–69. https://doi.org/10.1016/j.apcatb.2014.08.038.

(78) Reshetenko, T. V; Avdeeva, L. B.; Ismagilov, Z. R.; Chuvilin, A. L.; Ushakov, V. A. Carbon Capacious Ni-Cu-Al 2 O 3 Catalysts for High-Temperature Methane Decomposition. **2003**. https://doi.org/10.1016/S0926-860X(03)00080-2.

(79) Li, D.; Chen, J.; Li, Y.; Al, N.-C. /. Evidence of Composition Deviation of Metal Particles of a Ni-Cu/Al 2 O 3 Catalyst during Methane Decomposition to CO x-Free Hydrogen. *Int. J. Hydrogen Energy* **2008**, *34*, 299–307. https://doi.org/10.1016/j.ijhydene.2008.09.106.

(80) Klier, K.; Young, C.-W.; Nunan, J. G. Promotion of the Water Gas Shift Reaction by Cesium Surface Doping of the Model Binary Cu/ZnO Catalyst. *Zdrazll, M. Appl. Catal* **1986**, *25* (113), 432.

(81) Sun, J.; Cai, Q.; Wan, Y.; Wan, S.; Wang, L.; Lin, J.; Mei, D.; Wang, Y. Promotional Effects of Cesium Promoter on Higher Alcohol Synthesis from Syngas over Cesium-Promoted Cu/ZnO/Al 2 O 3 Catalysts. **2016**. https://doi.org/10.1021/acscatal.6b00935.

(82) Hadian, M.; Marrevee, D. P. F.; Buist, K. A.; Reesink, B. H.; Bos, A. N. R.; Bavel Van C, A. P.; Kuipers, J. A. M. Kinetic Study of Thermocatalytic Decomposition of Methane over Nickel Supported Catalyst in a Fluidized Bed Reactor. https://doi.org/10.1016/j.ces.2022.117938.

(83) Kvande, I.; Chen, D.; Yu, Z.; Rønning, M.; Holmen, A. Optimization and Scale-up of CNF Production Based on Intrinsic Kinetic Data Obtained from TEOM. *J. Catal.* **2008**, *256*, 204–214. https://doi.org/10.1016/j.jcat.2008.03.015.

(84) Snoeck, J.-W.; Froment, G. F.; Fowles, M. Kinetic Study of the Carbon Filament Formation by Methane Cracking on a Nickel Catalyst. *J. Catal.* **1997**, *169*, 250–262.

(85) Alstrup, I.; Tavares, M. T. Kinetics of Carbon Formation from CH4 + H2 on Silica-Supported Nickel and Ni-Cu Catalysts. *J. Catal.* **1993**, *139* (2), 513–524. https://doi.org/10.1006/JCAT.1993.1045.

(86) Kuvshinov, G. G.; Mogilnykh, Y. I.; Kuvshinov, D. G. Kinetics of Carbon Formation from CH4–H2 Mixtures over a Nickel Containing Catalyst. *Catal. Today* **1998**, *42* (3), 357–360. https://doi.org/10.1016/S0920-5861(98)00115-1.

(87) Thangaraj, A.; Eapen, M. J.; Sivasanker, S.; Ratnasamy, P. *Studies on the Synthesis of Titanium Silicalite, TS-1*; 1992.

Appendix 1: Details on the preparation of the used catalysts

	Atomic ratio Ni/promoter	Used $Ni(NO_3)_2 \bullet 6\ H_2O$ in 5 mL (g)	Promoter nitrate used in promoter stock (g)	Promoter stock used in the precursor (mL)	HNO_3 used in 5 mL precursor (µL)	Density precursor (g/mL)	GNP500 support used (g)	Precursor used (g)
Ni	n/a	5.0884	n/a	n/a	32.5	1.488	1.638	2.085
20NiLi	20	5.089	0.3030	1	32.5	1.482	1.260	1.504
10NiNa	10	5.088	0.3719	2	32.5	1.503	1.432	1.801
20NiNa	20	5.089	0.3719	1	32.5	1.473	1.495	1.834
30NiNa	30	5.090	0.3719	0.667	32.5	1.488	1.455	1.760
20NiK	20	5.089	0.4421	1	32.5	1.469	1.464	1.753
10NiMg	10	5.089	1.1217	2	32.5	1.509	1.433	1.692
20NiMg	20	5.089	1.1217	1	32.5	1.473	1.393	1.677
30NiMg	30	5.089	1.1217	0.667	32.5	1.487	1.427	1.771

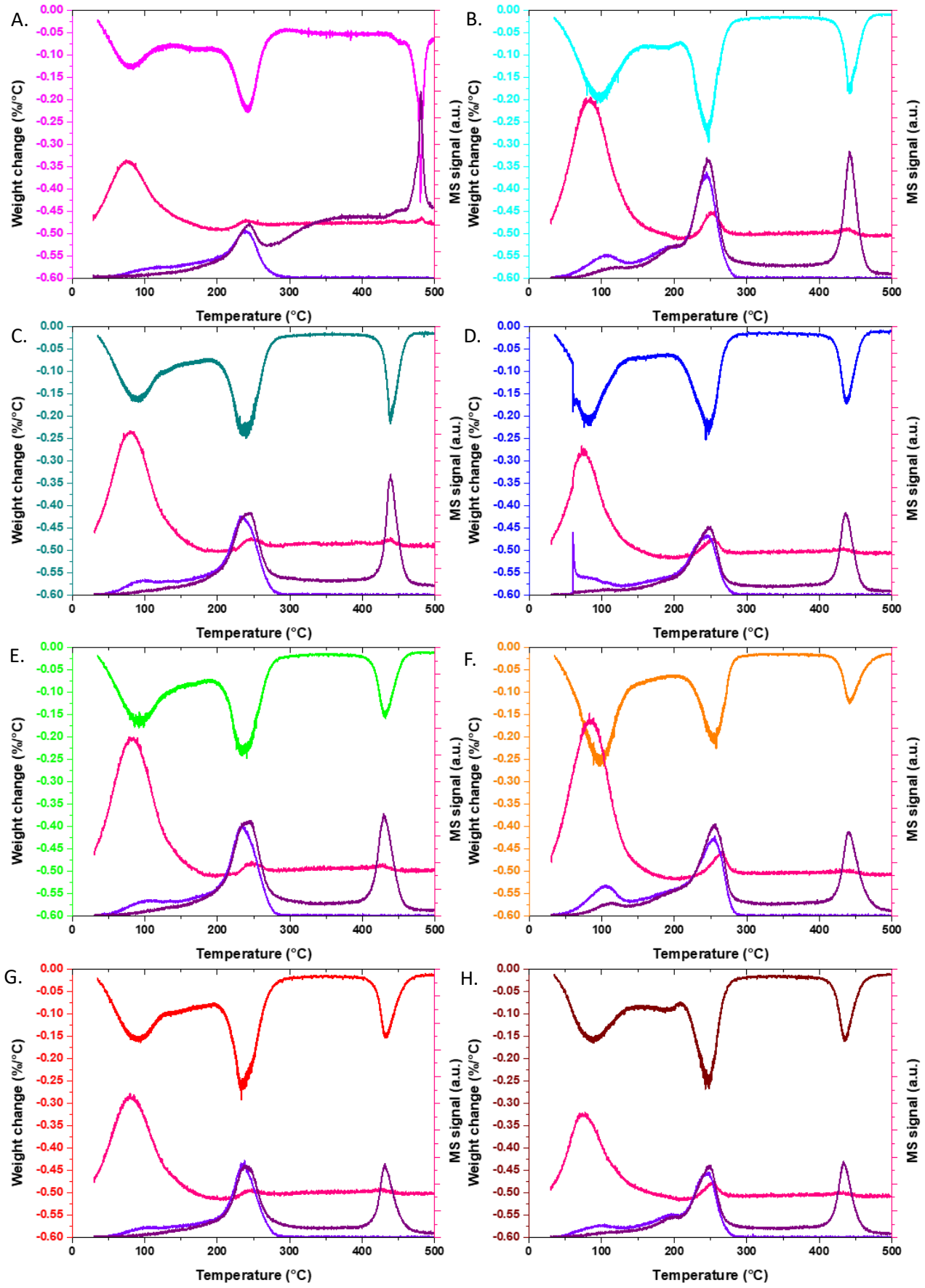

Appendix 2: TGA-MS profiles measured from 30 to 500 °C (5 °C/min) after impregnation and drying of the precursors on the support. On the left axis the change in sample weight and on the right axis the corresponding MS signals with M/Z 18 (H_2O) in pink, m/z 30 (NO) in light purple, and m/z 44 (N_2O/CO_2). A. 20NiLi, B. 10NiNa, C. 20NiNa, D. 30NiNa, E. 20NiK, F. 10NiMg, G. 20NiMg, H. 30NiMg

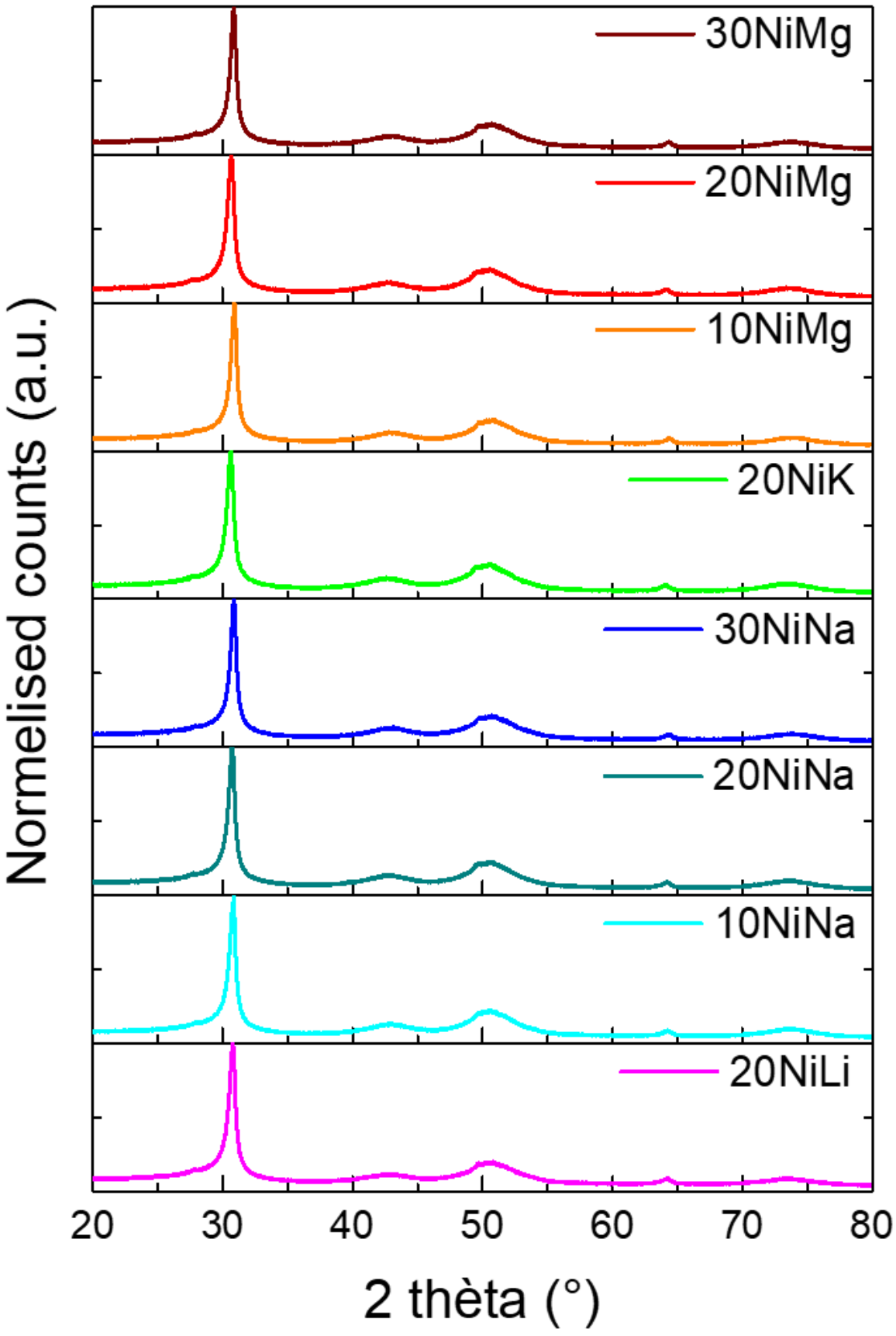

Appendix 3: Powder-XRD diffractograms of the used catalysts after heat treatment at 330 °C for 3h in 200 ml min^{-1} g^{-1} N_2 flow.

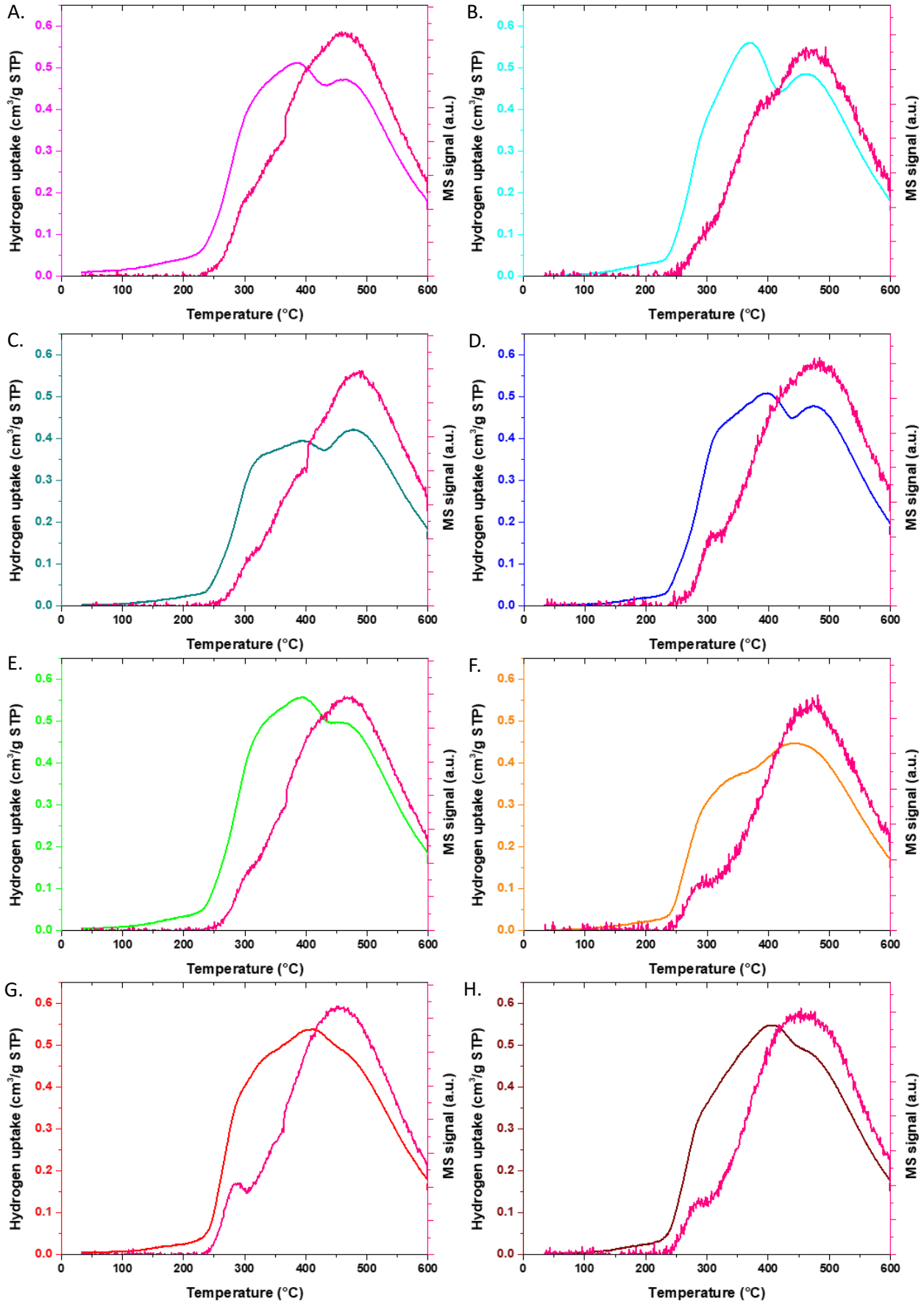

Appendix 4: TPR-MS profiles measured from 30 to 600 °C (5 °C/min) in 5% H_2/Ar at 200 mL min^{-1} g^{-1} after heat treatment of the catalysts. On the left axis the hydrogen uptake and on the right axis the methane (m/z 16) MS signal. A. 20NiLi, B. 10NiNa, C. 20NiNa, D. 30NiNa, E. 20NiK, F. 10NiMg, G. 20NiMg, H. 30NiMg

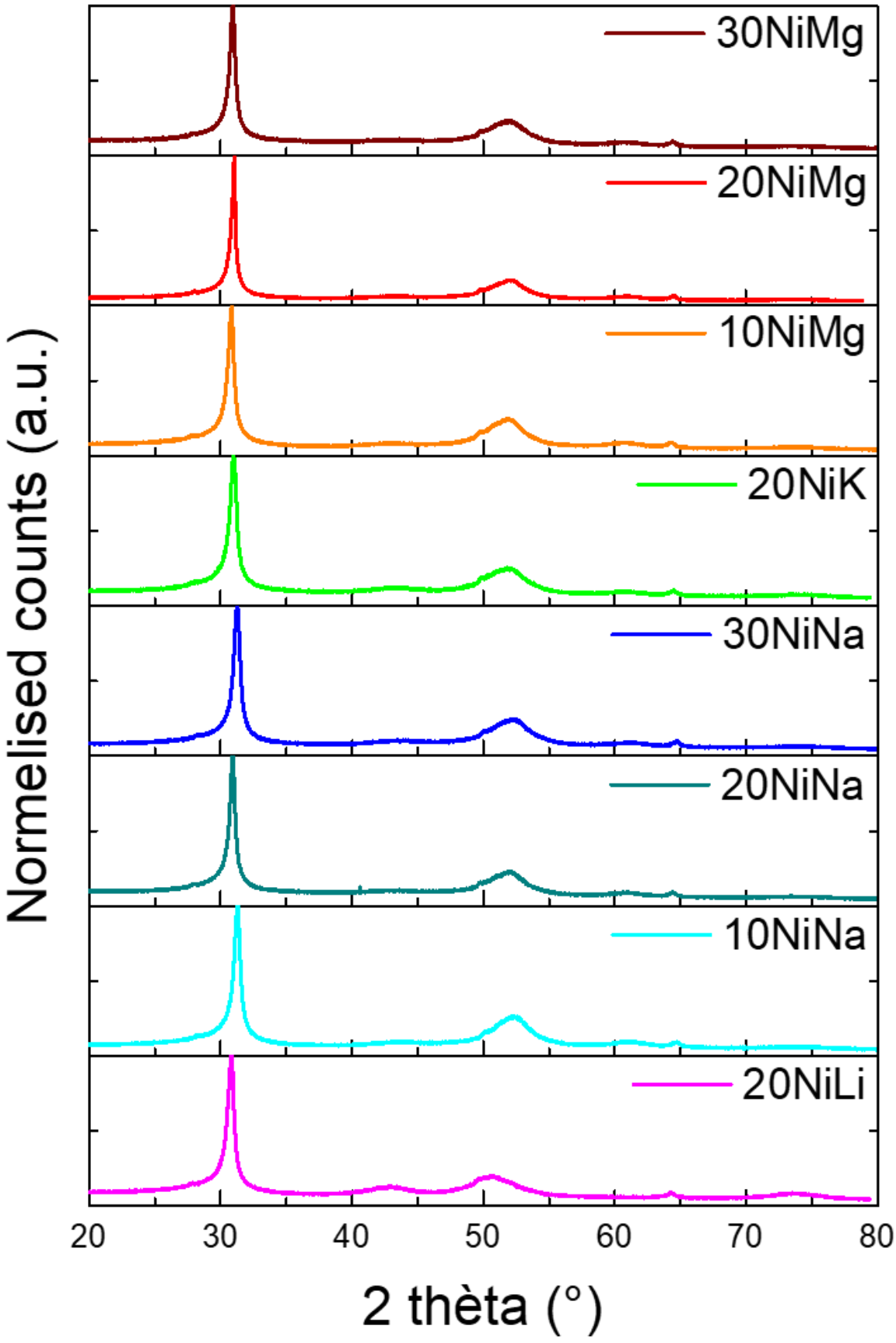

Appendix 5: XRD diffractograms measured after reduction at 350 °C for 3h in 5% H_2/Ar at 200 mL min^{-1} g^{-1} and passivation in air.

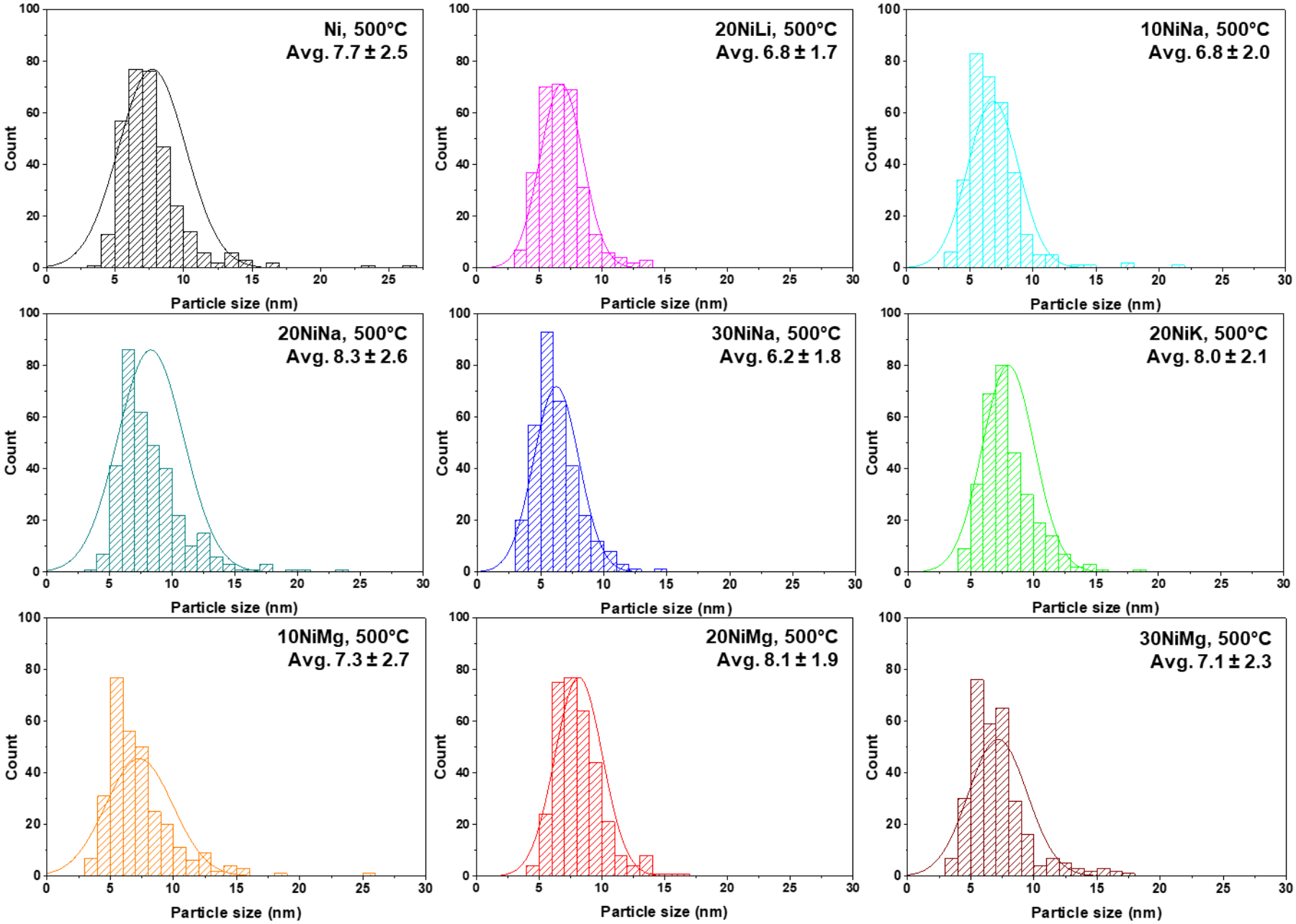

Appendix 6: Particle size distributions of catalysts prior to catalytic measurements at given temperatures, measured using TEM images. Given are the average measured particles sizes with their standard deviations.

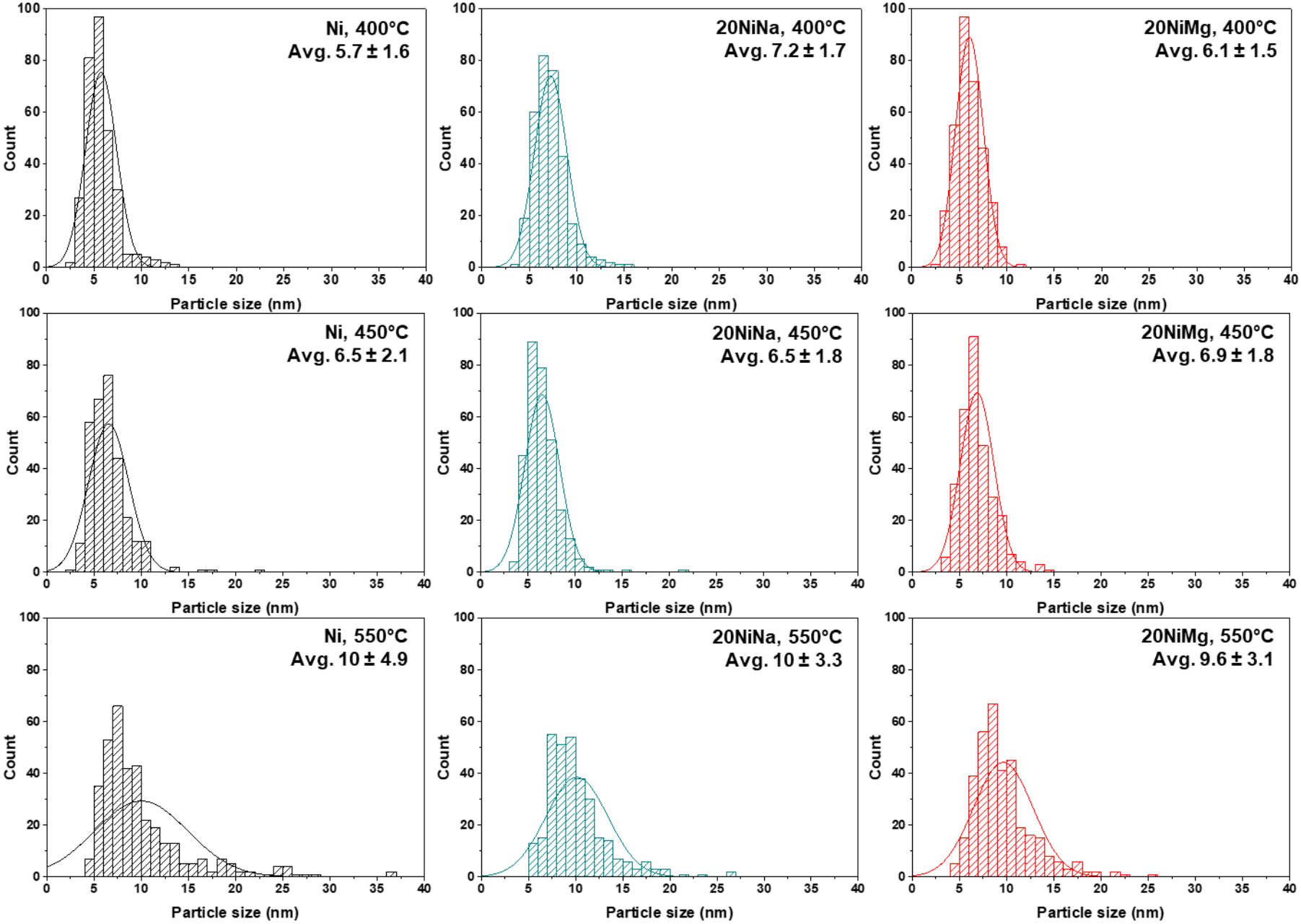

Continuation Appendix 6: Particle size distributions of catalysts prior to catalytic measurements at given temperatures, measured using TEM images. Given are the average measured particles sizes with their standard deviations.

A.

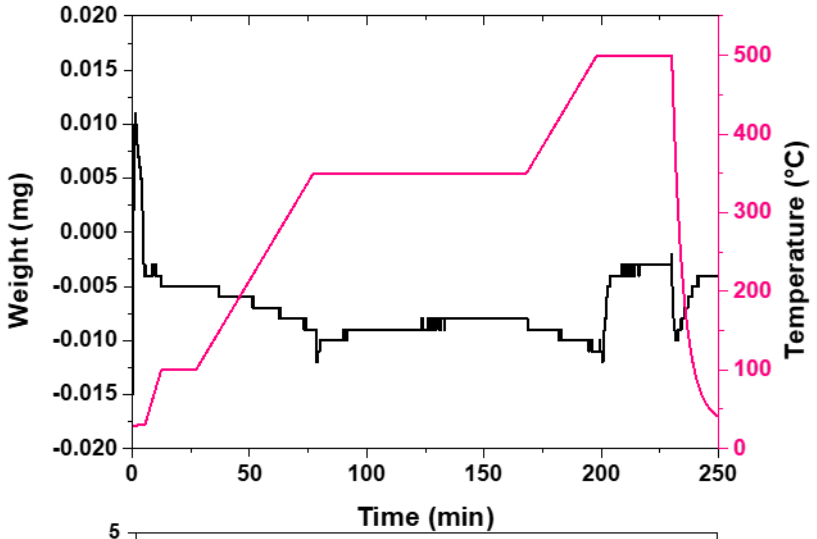

B.

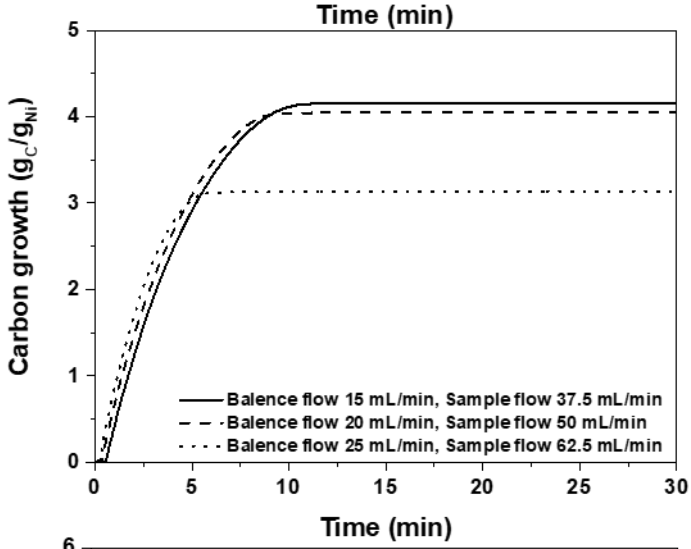

C.

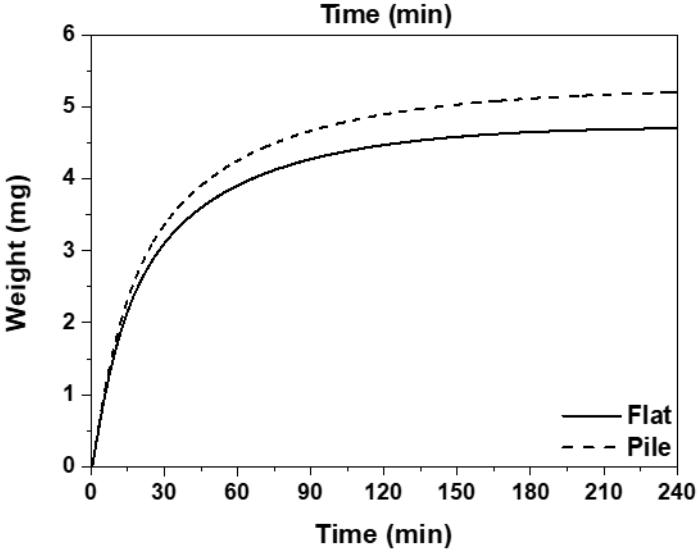

Appendix 7: Validity tests of catalytic measurements. A. weight changes of the empty sample pan during the whole catalytic program. B. Influence of the flow rates on the catalytic measurements using the Ni reference catalyst. Catalytic measurement was performed using 34% CH_4/Ar. C. Influence of loading manner on catalytic performance, with one sample flatly loaded over the bottom of the sample pan and the other loaded as a pile in the middle. Measurement was performed using a NiCu catalyst provided by Suzan Schoemaker.

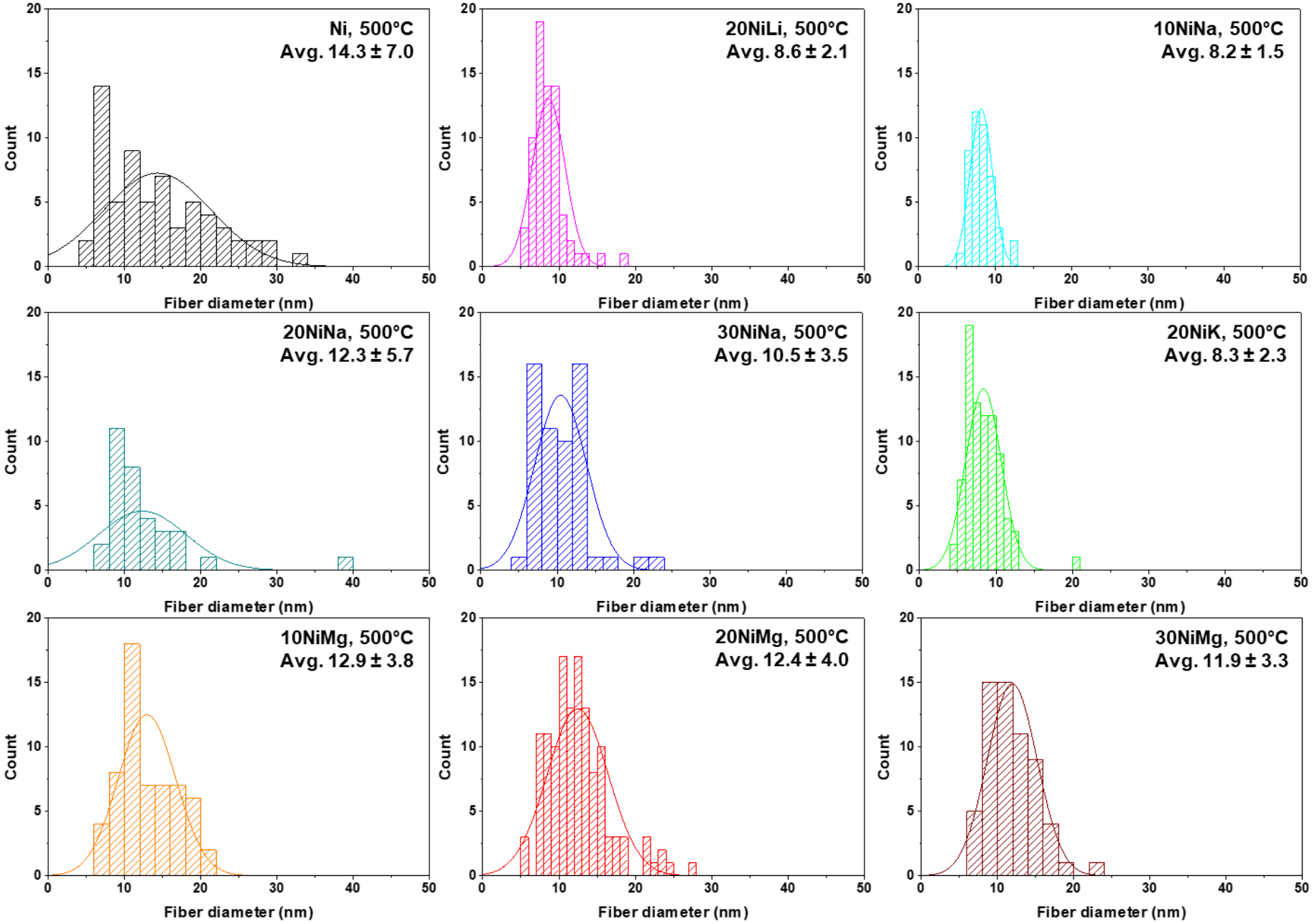

Appendix 8: Fiber diameter distributions of catalysts after catalytic measurements at given temperatures in 34% CH_4/Ar, measured using TEM images. Given are the average measured fiber diameters with their standard deviations.

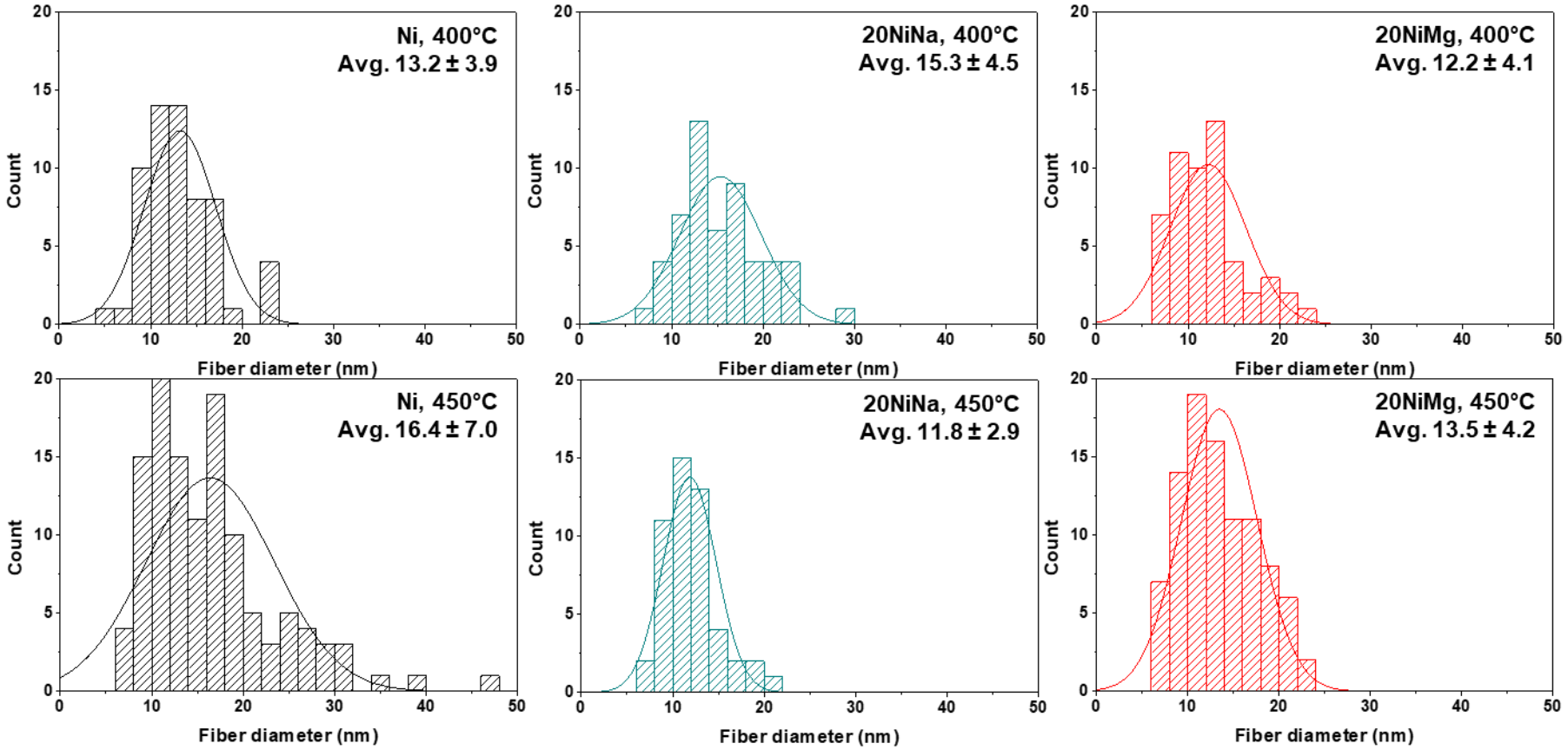

Continuation Appendix 8: Fiber diameter distributions of catalysts after catalytic measurements at given temperatures in 34% CH4/Ar, measured using TEM images. Given are the average measured fiber diameters with their standard deviations.